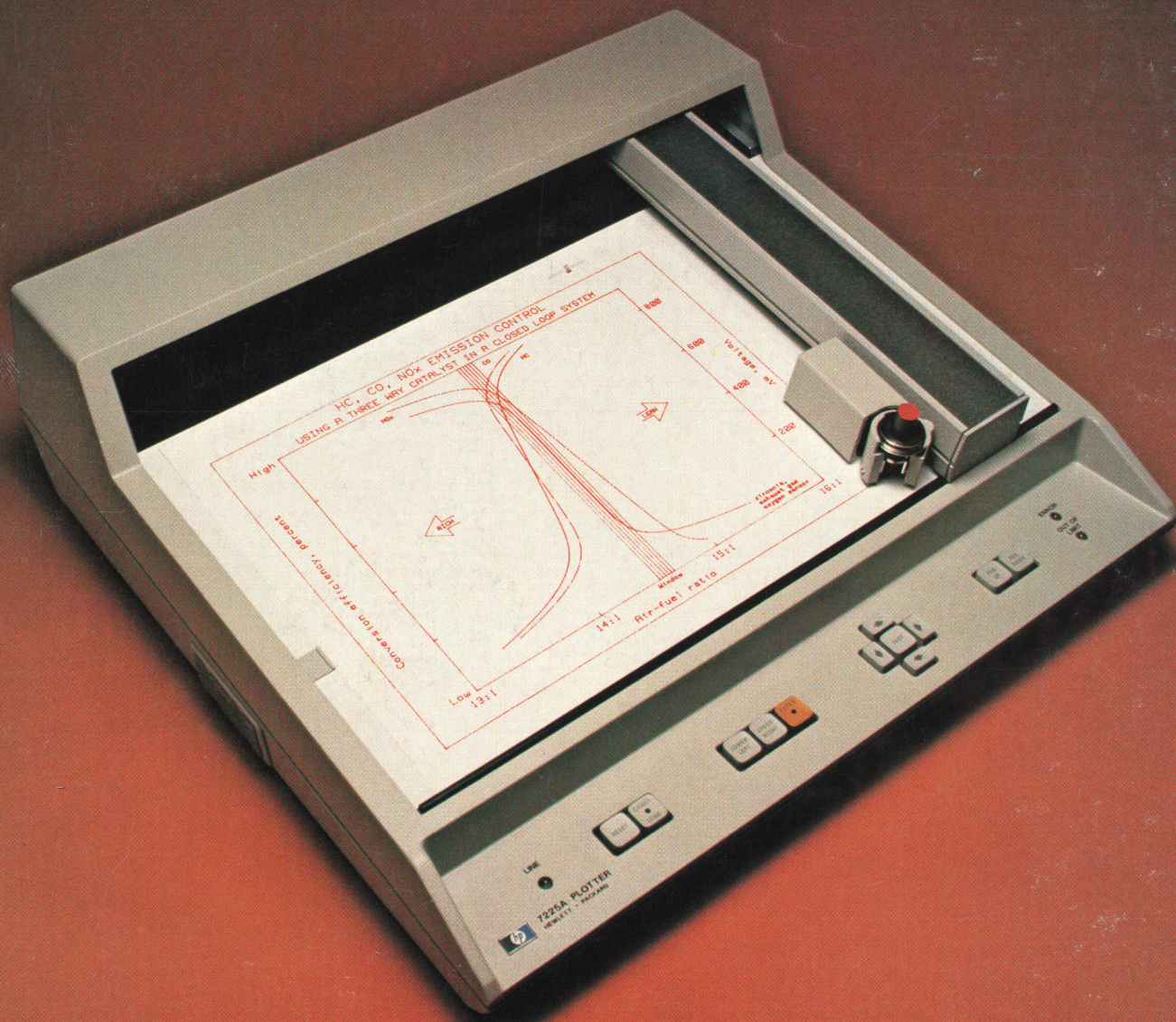


FEBRUARY 1979

HEWLETT-PACKARD JOURNAL



A High-Quality Digital X-Y Plotter Designed for Reliability, Flexibility and Low Cost

A new linear step motor design cuts costs and improves reliability without sacrificing line quality. Microprocessors and plug-in personality modules provide the flexibility.

by John A. Fenoglio, Bessie W. C. Chin, and Terry R. Cobb

MECHANICAL ADVANCES IN X-Y PLOTTERS have taken us from dc motors and slide-wire feedback to the more reliable open-loop rotary step motor drive systems. With the new HP Model 7225A Plotter, we are now entering the third generation of mechanical development. The design objectives for this new plotter emphasized the need of many users for a low-cost plotting solution. However, its lower cost had to be achieved while improving reliability and maintaining line quality.

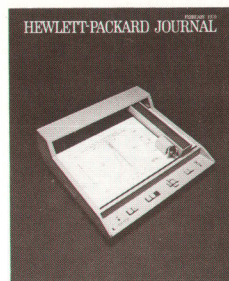
The 7225A (Fig. 1) is a dual-microprocessor plotter that produces high-quality plots on A4-size (8½×11 in) paper. It is available with several different interfaces to match most customers' applications. Fig. 2 shows examples of its plotting abilities.

Low Cost

Materials and labor are the primary factors that determine the cost of a product. Labor is especially critical because the total labor cost in a product is the direct labor cost times a rather large multiplier that includes manufacturing overhead. One way to reduce the labor content of a product is to invest in tooling. However, unless there is a prodigious market for a product, little tooling can be justified because of its high cost. To circumvent this, we decided to minimize the number of mechanical assemblies. The simplicity of linear step motor technology took us a giant step in that direction. Also helpful was the continuing drop in the cost of electronic components brought about by technological advances. This allowed us to place as much burden on the electronics as possible to help simplify the mechanics. With this approach we were able to reduce assembly and test times for the 7225A by a factor of six compared to other similar products.

The main emphasis in the electronics development was to keep the parts count down. This is important because of the time required to load parts onto printed circuit boards. The microprocessor selected provides the RAM, ROM, and latched I/O ports all in a single 40-pin package. The plotter's electronic circuitry is all located on a single board. This reduces the cost of

connectors and assembly time. To further reduce assembly and test time, the plotter is designed to operate without any electrical adjustments.



Cover: Model 7225A Plotter is a reliable, low-cost digital X-Y plotter that is expected to make computer graphics practical in many applications where graphics capability has been considered too expensive. Plug-in personality modules adapt a single mainframe to different input/output requirements.

In this Issue:

- A High-Quality Digital X-Y Plotter Designed for Reliability, Flexibility and Low Cost, by John A. Fenoglio, Bessie W.C. Chin, and Terry R. Cobb* **page 2**
- Linear Step Motor Design Provides High Plotter Performance at Low Cost, by Lung-Wen Tsai and Robert L. Ciardella* **page 7**
- Developing a Low-Cost Electrostatic Chart-Hold Table, by Alec J. Babiarz,* **page 10.**
- Simple, Efficient Electronics for a Low-Cost X-Y Plotter, by William G. Royce and Peter Chu* **page 14**
- A Closed-Loop System for Smoothing and Matching Step Motor Responses, by Philip P. Maiorca and Norman H. MacNeil* **page 18**
- Multi-Frequency LCR Meters Test Components under Realistic Conditions, by Kohichi Maeda and Yoh Narimatsu* **page 24**

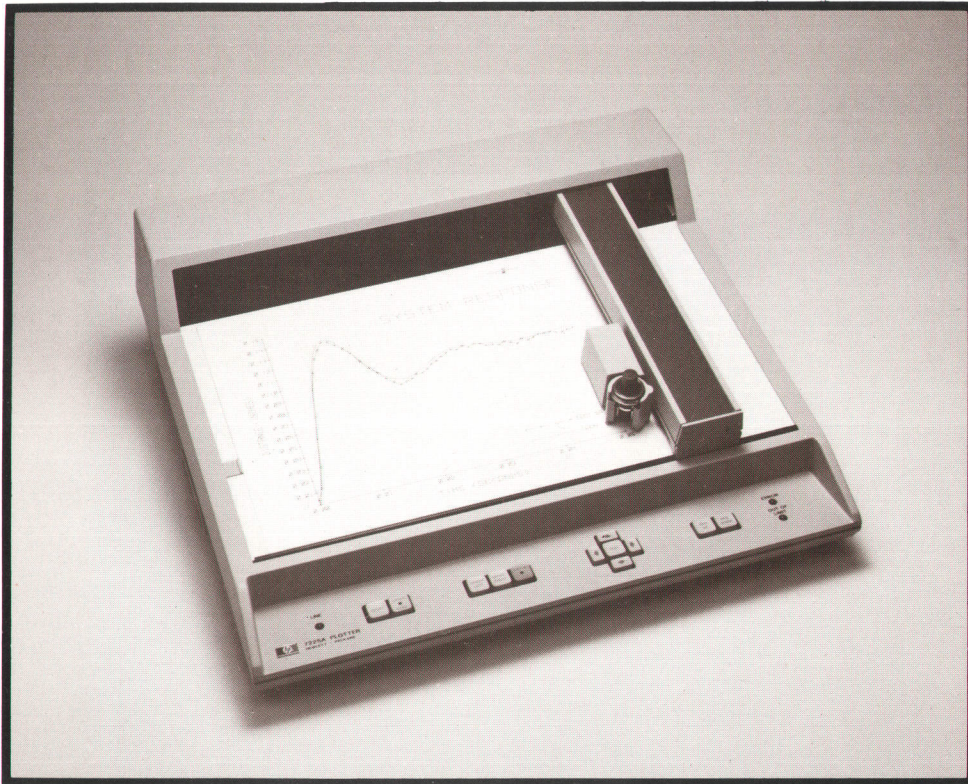


Fig. 1. Model 7225A Plotter produces high-quality plots on A4-size (8½×11 in) paper. Its linear step motor design delivers twice the reliability of older plotters at about half the cost. Personality modules adapt the plotter to different interfaces.

Typically high power and high cost go together, so another important technique for reducing cost is to reduce the power requirements. The motor drivers satisfy this need. They are class D switching amplifiers that offer substantial power reduction compared with linear amplifiers. The plotter's power supply is extremely simple, using a transformer with a single secondary winding.

Reliability

A true low-cost plotting solution requires not only that the purchase price be low, but also that the continuing cost of ownership be low. This means high reliability and low repair cost. Fortunately, the items that lower the manufacturing cost also improve reliability and serviceability, since a mechanically simple mechanism provides inherent reliability. The only moving parts associated with the X-Y mechanics are the ball bearings that support the motors. This has resulted in a demonstrated life expectancy greatly exceeding that of previous plotters.

The electronic objective of reduced parts count also contributes to a lower failure rate. The concern for power reduction results in lower internal temperatures, which help prolong the life of electronic components. These factors, coupled with a very conservative design approach, produce higher reliability. The annual failure rate of the 7225A has been reduced by a factor of two compared to the product it replaces.

Even so, all things must someday fail, and to reduce repair cost, it is important to minimize the time re-

quired to repair the item. Repair time can be divided into the time needed to diagnose the problem and that needed to correct it. The effort put into reducing assembly time directly reduces replacement time, and

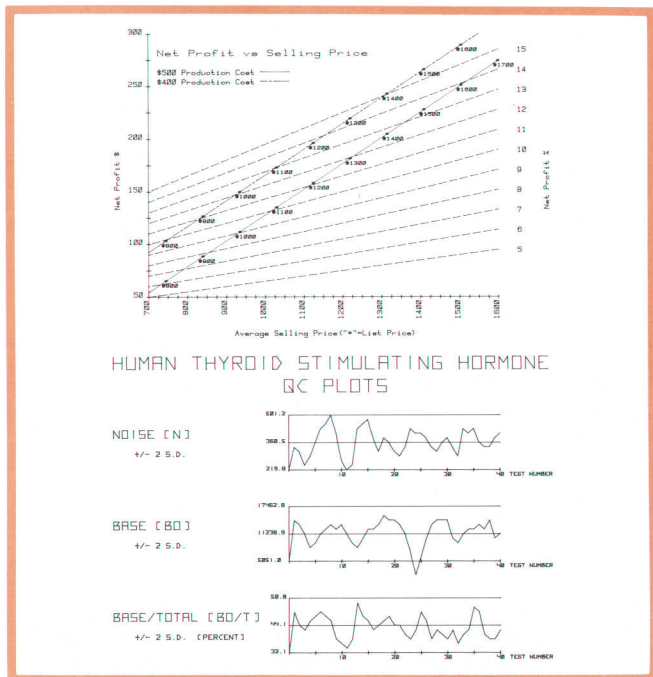


Fig. 2. Model 7225A draws continuous lines at 250 mm/s in each axis and draws text at up to three characters per second. 0.032-mm microsteps result in smooth, visually continuous lines.

several aids are provided to help reduce diagnostic time. An external confidence test switch initiates a test that exercises most of the circuitry and mechanics to aid in isolating problems. Further fault isolation assistance is provided by designing the plotter to support signature analysis troubleshooting techniques.

Quality

Price/performance trade-offs can be made during the design of any product. The quality of the marks placed on paper by a plotter is its most important parameter. A true bargain exists when the price can be lowered without sacrificing line quality.

The 7225A Plotter has several features that help ensure good lines. First, there are no cumulative errors in the linear step motor approach, nor are there any pulleys, whose diameter and concentricity tolerances contribute a major source of error. Also eliminated are cables and the errors caused by their stretching when the pen carriage accelerates. Line quality is further enhanced by adding dynamic velocity feedback to the servo system. Custom hybrid accelerometers sense perturbations in motor movement and supply correcting error signals. A microstep drive signal technique is employed to divide the basic 1-mm step size of the motor into 32 equal sub-steps. This produces smooth, continuous lines at all angles (see Fig. 2).

Flexibility

The requirements for a plotter vary considerably depending on the customer's needs. In the past it has been necessary to provide several different plotters to meet all the needs. Plotter characteristics that usually change are the interface hardware, the command syntax and language, and software features. The modular approach of this new generation of plotters satisfies these requirements with only one mainframe. A microprocessor in the mainframe controls pen movement and monitors the front panel. An interfacing module called the personality module provides the needed flexibility. The personality module is a microprocessor-based plug-in card that contains the hardware connectors appropriate to the selected interface. It also contains the language interpreter that defines the instructions used to control the plotter. Any extra features and capabilities of the plotter, such as internal character generation and dashed-line drawing, reside on this plug-in. A customer can select a very simple parallel interface with only move and pen up/down capabilities, and then, as needs change, replace it with a more complex personality module that supports the HP-IB (Hewlett-Packard Interface Bus*), interprets HP-GL (Hewlett-Packard Graphics Language), and contains a full set of graphics features. This concept also makes it easy to provide fu-

*IEEE 488, ANSI MC1.1.

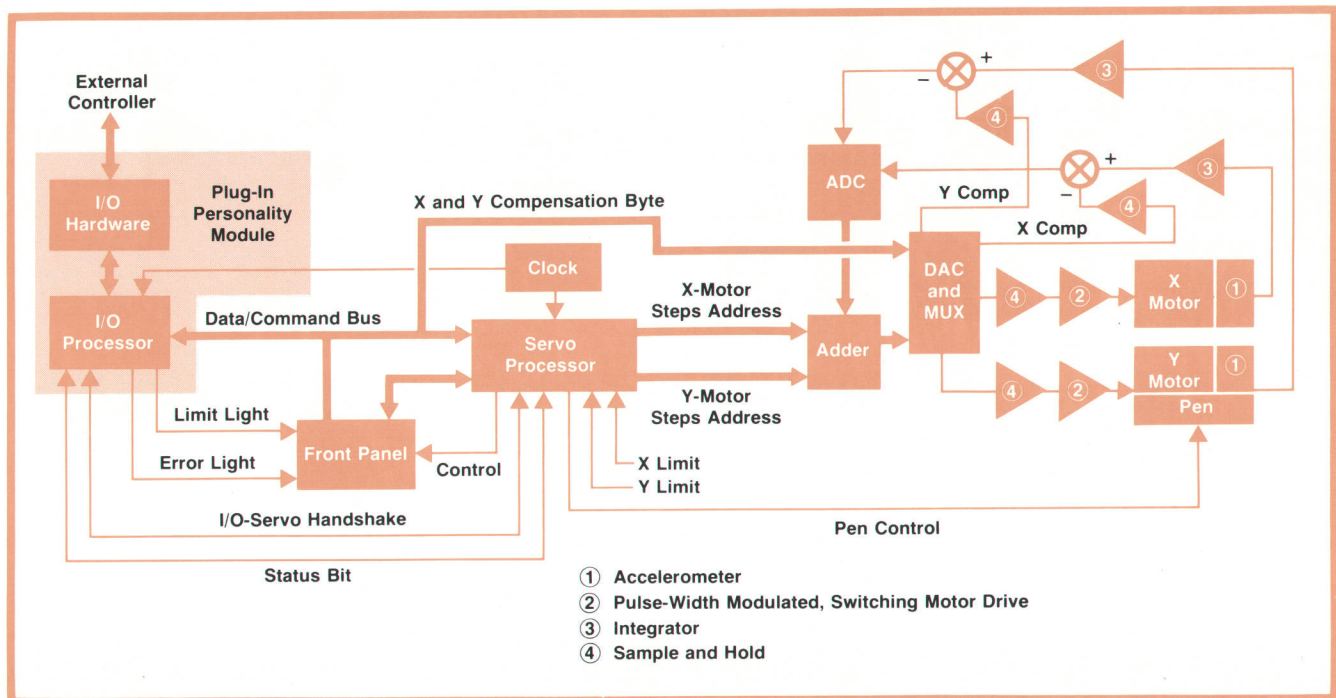


Fig. 3. Model 7225A block diagram. Two microprocessors, one in the mainframe and one in the personality module, control all functions. Each motor module contains a specially designed accelerometer that provides motor-movement feedback.

ture interfaces as new products and customers require them.

Block Diagram

Fig. 3 is a block diagram of the 7225A Plotter. The basic mechanism consists of two linear step motors. Each motor module contains a specially designed hybrid accelerometer that senses motor movements. The control system integrates the accelerometer signal to provide velocity feedback.

The remainder of this article discusses the functions of the two microprocessors and the various personality modules. The motor and platen designs are described in the article on page 7. The electronic design is the subject of the article on page 14. The servo and accelerometer story begins on page 18.

Servo Processor

The processor in the 7225A mainframe is called the servo processor. It directly controls the X-axis and Y-axis motors, the pen, and the chart hold. It responds to inputs either from the front panel or from the personality module. It also performs general mainframe housekeeping chores.

The servo processor is a single-chip 3870 with its own internal program ROM and RAM and four eight-bit I/O ports. Two of the ports provide a five-bit step address to the circuits that position the motors. Another port is used as a data/command bus to the personality module. This port is shared with the front panel, and during moves it provides a compensation byte to the acceleration-deceleration electronics. The fourth port, along with extra pins on the first two ports, provides handshake lines to the personality module, other front-panel inputs and outputs, pen control, chart load control, and X and Y limit inputs. A status line from the servo processor informs the personality module when a front-panel input changes the mainframe's status.

The front-panel inputs come from pushbuttons that are pressed by the operator. The operator can move the pen over the full platen surface at two speeds, go to or set either lower left or upper right scaling points, enter a digitized point, turn chart hold on or off for paper loading, raise or lower the pen, reinitialize the plotter, or reset the plotter to a power-up condition.

When a position move is requested either by the front panel or the personality module, the servo processor calculates the number of steps required for acceleration, deceleration, and slew. Before the first step, the maximum velocity for each axis is determined and used to output a compensation byte during acceleration and deceleration. Once the servo processor begins execution of the move, all inputs are ignored with the exception of a cursor move. During a

cursor move the front panel is continually monitored once the X and/or Y motors have reached a constant velocity.

As the servo processor begins the move, the five-bit X and Y motor step address is incremented or decremented using a vector algorithm. The time between each step follows a fixed profile during acceleration and deceleration, and is a constant 125 microseconds during slew. The processor maintains a step count for branching from acceleration to slew to deceleration to a complete stop. At the completion of the move and any associated pen maneuver, the servo processor returns to its idle loop and waits for new inputs.

I/O Processor

The processor in the personality module, if required, is called the I/O processor. It translates commands from an external controller to the servo processor. The I/O processor controls the actions of the servo processor using eight commands (Fig. 4). At the start of a conversation between the two processors the I/O processor first indicates its readiness. The servo processor responds, after completing any previous operation, with a status byte on the data/command bus. The status byte indicates the pen state, a change in scale limits, the digitize state, the chart hold state, and whether a front-panel reset has occurred. The I/O processor accepts the status byte, determines whether the status affects the next command, and outputs the command to the servo processor.

The commands force the servo processor to execute various routines, either outputting data, accepting input data, or returning to its idle loop. With these commands the I/O processor can instruct the servo

Command	Servo Processor Action
Null	Return to Idle Loop
Position and Pen	Accept Five Bytes for Position Move and/or Pen Maneuver
Initialization	Initialize Plotter to Power-Up Condition
Set P1, P2	Accept Eight Bytes Setting New Scale Limits
Enable Digitize	Turn on Enter Light and Store Present Position as Digitize Point when Operator Presses Enter Button
Disable Digitize	Exit Digitize Mode
Output Present Position and P1, P2	Output Four Bytes Reflecting Position and Eight Bytes of Current Scale Limits
Output Digitize Point	Output Five Bytes of Last Stored Digitized Point and Pen Status

Fig. 4. I/O processor (in personality module) controls the actions of the servo processor (in mainframe) using eight commands. Commands from an external controller are translated by the I/O processor into these eight commands.

SPECIFICATIONS

HP Model 7225A Plotter

PLOTTING AREA

Y AXIS: 203 mm (8 in)
X AXIS: 285 mm (11.2 in)
Accepts up to ISO A4 or 8½ × 11-in chart paper.

PLOTTING ACCURACY: ±0.25 mm (0.01 in) [includes linearity and repeatability and assumes the plotter has been "zeroed" exactly to the lower left (0,0) coordinates].

REPEATABILITY: 0.1 mm (0.004 in) from any given point and direction.

ADDRESSABLE STEP SIZE: 0.032 mm (0.0013 in) smallest addressable step.

PEN VELOCITY

250 mm/s (10 in/s) in each axis,
350 mm/s (14 in/s) on 45° angle.

VECTOR LENGTH: No limit—any length vector within the plotter's mechanical limits will be plotted.

CHARACTER PLOTTING SPEED: Up to 3 character/s for 2.5-mm (0.1-in) characters.

POWER REQUIREMENTS

SOURCE: 100, 120, 220, 240V -10%, +5% internally selectable.
FREQUENCY: 48-66 Hz.
CONSUMPTION: 70 W maximum.

ENVIRONMENTAL RANGE

TEMPERATURE: 0°C to 55°C.
RELATIVE HUMIDITY: 5% to 95% (below 40°C).

DIMENSIONS:

SIZE: 140 mm H × 413 mm W × 379 mm D (5.5 in H × 16.3 in W × 14.9 in D).
NET WEIGHT: 8 kg (17.6 lb).

Personality Modules

(One Required)

17600A PERSONALITY MODULE: The 17600A Personality Module adapts the 7225A Graphics Plotter to a wide range of desktop computers. Available for use with the 9815A, 9820A, 9821A, 9825A, and 9830A/B Computers with the general I/O interface, this module decodes commands from the computer and sends positioning and pen status commands to the plotter mechanics. Additional cir-

cuitry has been included to work with the plotter confidence test electronics to verify proper operation of the plotter with the Personality Module installed.

The 7225A equipped with a 17600 Personality Module is plug-to-plug interchangeable with the 9862A Plotter. The basic plotting functions of absolute and relative coordinate moves and pen raising and lowering are further enhanced by the user's choice of an HP desktop computer.

17601A PERSONALITY MODULE: The 17601A Personality Module adapts the 7225A Graphics Plotter to desktop computers, computer systems, or intelligent instrument systems which use the Hewlett-Packard Interface Bus, HP-IB (IEEE 488-1975). Using the high-level instruction set called Hewlett-Packard Graphics Language (HP-GL), 38 instructions are available for vector plotting, character set and line type selection, point digitizing, user-unit scaling, and labeling with programmable size, slant, and direction of characters.

The 17601A Personality Module is software compatible with the 9872A Graphics Plotter. In addition, the 17601A allows the 7225A to operate in a "listen-only" mode, making the plotter ideal for operation with computer-based systems.

17602A PERSONALITY MODULE: The 17602A Personality Module adapts the 7225A Graphics Plotter for use with calculators, computers, or intelligent instrument systems. The 17602A Personality Module controls the basic plotting functions of absolute and relative coordinate moves and pen raising and lowering and provides plug-to-plug interchangeability with the HP 7210A Plotter.

This module has the designed-in flexibility to interface with 8, 12, or 16-bit controllers. In addition, the position data can be 4 or 8-bit words coded in BCD or Binary.

All control panel pushbutton logic is available at the rear panel connector to allow use with remote plotter controllers. Additional circuitry has been included to work with the plotter confidence test electronics to verify proper operation of the plotter with the personality module installed.

PRICES IN U.S.A.:

7225A Plotter, \$1850. 17600A Personality Module, \$150. 17601A Personality Module, \$750. 17602A Personality Module, \$200.

MANUFACTURING DIVISION: SAN DIEGO DIVISION

16399 West Bernardo Drive
San Diego, California 92127 U.S.A.

processor to perform position moves and pen maneuvers, enter or exit the digitizing mode, set scale limits, or perform a power-up reset. The I/O processor can also have the servo processor output its current position, the scaling limits set by the front panel, and any digitized point entered from the front panel. Any data transfer occurs after the servo processor accepts the command. Upon completion of the transfer the servo processor executes the current maneuver, if any and returns to its idle loop.

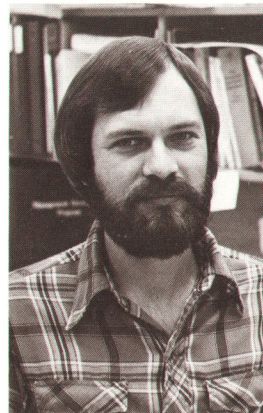
While the servo processor is executing the current move the I/O processor can receive the next command from the controller. Depending on the interface language and the command, several actions may take place in the I/O processor, but generally the outcome is a new command to the servo processor. Features such as characters and dashed lines require the I/O processor to generate a series of position moves and pen maneuvers to the servo processor.

The position data sent to the servo processor is in absolute X and Y plotter units, giving the I/O processor complete position control of the X and Y motors. Because of this the I/O processor continually monitors the status byte for any changes from the front panel, since a change of scale limits, for example, can determine the size and rotation of characters, dash pattern lengths, and user scaling units. The level of interaction depends on the characteristics of the personality

module, but the primary result is that the personality module translates the various user languages to marks on the paper.

Acknowledgments

The authors would like to thank Dan Allen and Nilesh Gheewala for their project leadership. Also Don Hiler for the product design and Bill Wigand for production engineering. Special thanks go to the many people throughout the HP San Diego Division for their help in making this product possible. 



Terry R. Cobb

An HP employee since 1974, Terry Cobb was responsible for the processor architecture and the general purpose and HP-IB personality modules for the 7225A Plotter. Terry received his BSEE degree in 1973 and his MSEE degree in 1975 from the University of Texas at Arlington. Born in Ft. Worth, Texas, Terry is also a 1969 Vietnam War veteran. Terry, his wife, and their two children live in Escondido, California. Camping, water skiing, body surfing, racquetball, and basketball keep Terry busy in his off-hours.



John A. Fenoglio

John Fenoglio received his BSEE degree in 1972 from California State Polytechnic University at Pomona and his MSEE degree in 1974 from California State University at San Diego. An HP employee since 1972, John was project leader for the 7203A Graphic Plotter and project manager for the software and electronics of the 7225A Plotter. He is married, lives in San Diego, California, and spends much of his spare time water skiing, snow skiing, doing amateur radio "moon bounce"

communications, and flying his Piper Comanche airplane, often as far as the Carribean, Central American, and South American regions.



Bessie W.C. Chin

An HP employee since 1974, Bessie Chin was responsible for the 7225A Plotter firmware development, including the servo processor firmware and the general processor and HP-IB personality modules. Bessie received her BA degree in information science in 1973 from the University of California at San Diego and her MS degree in computer science in 1974 from the University of California at Berkeley. Born in Hong Kong, Bessie is single and lives in San Diego, California, with

her five-pound poodle. Landscaping, Chinese cooking, jazz exercise, and skydiving keep Bessie busy in her off-hours.

Linear Step Motor Design Provides High Plotter Performance at Low Cost

by Lung-Wen Tsai and Robert L. Ciardella

THE MOTORS DESIGNED for the 7225A Plotter are four-pole, two-phase, permanent magnet linear step motors. Operation of the linear step motor is well covered in the literature.¹ The motor has two basic parts: a rectangular steel bar called the stator, and a magnet-electromagnet assembly called the mover. The stator (Fig. 1) is made of C1018 cold-rolled steel bar with C1010 cold-rolled steel sheet metal laminated on top of it. The sheet metal is etched with equidistant rectangular teeth. The centerline distance between two adjacent teeth is called the pitch, L .

The mover consists of two electromagnets and a permanent magnet between them as shown in Fig. 2. The permanent magnet serves as a bias source. Each electromagnet has two poles, and each pole has the same number of teeth. The pole phase relationship is such that pole 4 lags pole 1, pole 2 lags pole 4, and pole 3 lags pole 2 by one-quarter pitch in each case. This is depicted in Fig. 2.

The permanent magnet flux path is through the electromagnets, across the air gap between the electromagnets and the stator, and through the stator. In

the absence of electromagnet currents, the permanent magnet provides nearly equal and constant flux to all poles. The direction of the flux across each air gap is shown in Fig. 2b. Under this condition, there is no tangential force and the mover is free to stay at any arbitrary position.

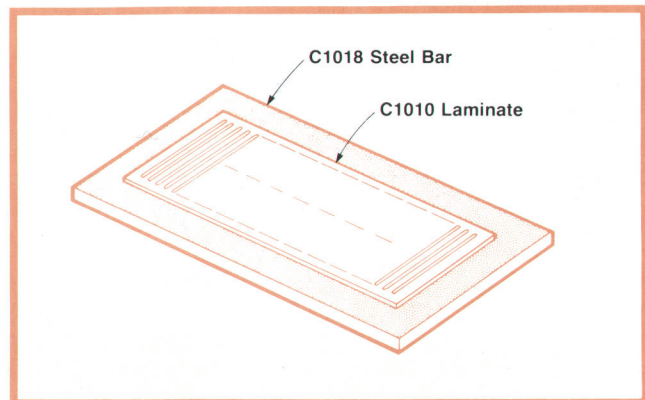


Fig. 1. Linear step motor stators are made of cold-rolled steel bar with cold-rolled sheet metal laminated on top. Teeth are etched into the sheet metal.

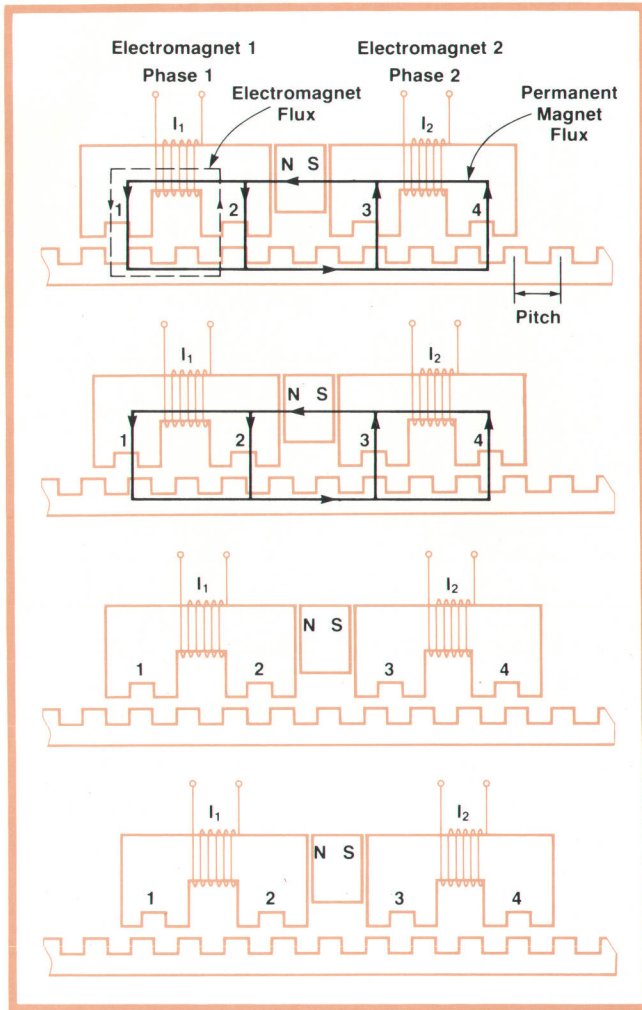


Fig. 2. Linear step motor mover consists of two electromagnets with a permanent magnet between them. By selectively energizing the electromagnets the mover is induced to move in steps. It takes four steps to move one pitch, the centerline distance between adjacent stator teeth.

When one of the electromagnets, say number 1, is fully energized, the applied current switches the flux entirely into one pole, say pole 1, of electromagnet 1 as shown in Fig. 2a. This brings the flux density in air gap 1 to a maximum, say 20 kilogauss, and the flux density in air gap 2 to nearly zero. The mover then repositions itself until the teeth in pole 1 line up with those of the stator. Similarly, energizing pole 4 to 20 kilogauss causes the mover to take a new position as shown in Fig. 2b, energizing pole 2 causes the mover to take a new position as shown in Fig. 2c, and energizing pole 3 causes the mover to take a new position as shown in Fig. 2d. The sequence is completed with a fourth energization that brings the mover to a new position one pitch away from its initial position.

The pitch of the motor designed for the 7225A Plotter is 1.016 mm (0.040 in). Therefore, each step is 0.254 mm (0.010 in). Finer resolution in step size is achieved by applying currents to both electromagnets

simultaneously and balancing them. This is called interpolation.

To interpolate, a sinusoidal current is applied to electromagnet 2 and a cosinusoidal current to electromagnet 1. The tangential force developed by pole 1 is given by:

$$F_1 = -\phi_1^2 \frac{\partial R_1}{\partial X} \quad (1)$$

where ϕ_1 denotes the total flux across air gap 1, R_1 denotes the air gap reluctance, and X is the position of the mover with respect to the stator.

For a first-order approximation, assume that the flux across air gap 1 that is contributed by the permanent magnet is ϕ_m (constant), and that the air gap reluctance, neglecting higher harmonics, is given by

$$R_1 = R_0 - r \cos \frac{2\pi X}{L} \quad (2)$$

where R_0 is the average reluctance, r is the first harmonic in the reluctance, and L is the pitch. The air gap reluctances in poles 2, 3, and 4 may be obtained in a similar manner, with appropriate phase changes.

The applied currents take the following forms:

$$I_1 = I_0 \cos \left(\frac{2\pi X_i}{L} \right) \quad (3)$$

$$I_2 = I_0 \sin \left(\frac{2\pi X_i}{L} \right) \quad (4)$$

where X_i denotes the desired input position. Thus the total flux across air gap 1 is given by:

$$\phi_1 = \phi_m \left(1 + \cos \frac{2\pi X_i}{L} \right) \quad (5)$$

I_0 is chosen so that

$$\phi_m = \frac{NI_0}{2R_0} \quad (6)$$

and N is the number of turns in each coil.

Substituting equations 2 and 5 into 1, we obtain

$$F_1 = -\left(\frac{2\pi r}{L} \right) \phi_m^2 \left(1 + \cos \frac{2\pi X_i}{L} \right)^2 \sin \frac{2\pi X}{L} \quad (7)$$

The tangential forces developed by poles 2, 3, and 4 may be obtained in a similar manner. Summing all four components, the total tangential force is:

$$F = - \left(\frac{2\pi r}{L} \right) \phi_m^2 \sin \left[\left(\frac{2\pi}{L} \right) (X - X_i) \right] \quad (8)$$

This equation shows that for every input X_i , the motor always has an equilibrium position $X = X_i$. When the mover is displaced away from its equilibrium position, the motor will generate a restoring force that is a sinusoidal function of $X - X_i$. The maximum restoring force is given by

$$F_{\max} = \frac{2\pi r}{L} \phi_m^2 \quad (9)$$

As the applied currents are advanced by an amount corresponding to an increment ΔX_i , the mover advances an increment $\Delta X = \Delta X_i$. Theoretically, it is possible to advance the mover by infinitesimal increments and position the mover at any desired location on the stator. In practice this is limited by the available hardware and software. For the 7225A Plotter, a step size of 0.032 mm (0.00125 in) is used.

Interpolation Error

The force equation, equation 8 above, is based on the assumption that the reluctance in the iron path, the leakage flux, and the higher harmonics of the air gap reluctance are negligible. It is also based on the assumption that perfect drive currents, as given by equations 3 and 4, are applied. In practice, to obtain high force, one always designs the motor to operate at high flux density, which reduces the permeability of the iron to the point where the reluctance of the iron path can no longer be neglected, and where the leakage flux can no longer be neglected. Iron saturation in the tooth area also introduces distortions in the flux paths across the air gap, affecting the harmonic content of the air gap reluctance. The reluctance of the air gap depends on the tooth shape of the pole pieces, the pitch, the actual air gap, the materials used, and the flux level.^{2,3} The actual tooth shape, pitch, and air gap depend on design and manufacturing tolerances.

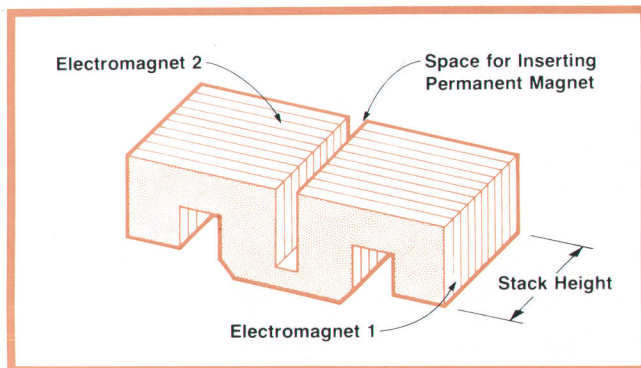


Fig. 3. Mover pole pieces are made of a stack of laminations.

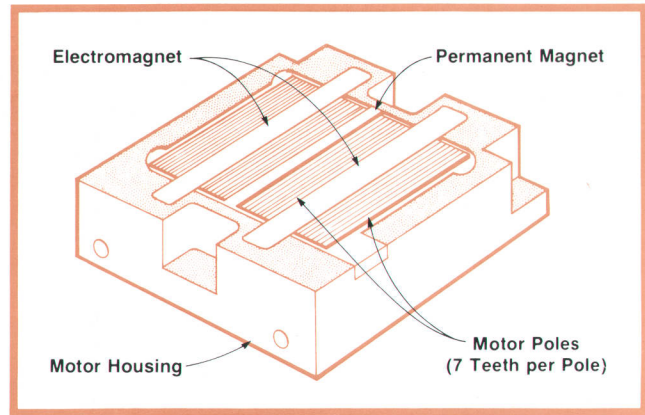


Fig. 4. Completed mover. Any assembled mover can be placed on any stator to form a motor.

Tolerances in the electronics introduce deviations in the applied currents that affect the flux level in the air gap.

Since all of the factors mentioned above affect the flux distribution and therefore the balance of forces among the four poles, the equilibrium position X for the mover is not at X_i , in general. The difference between the actual equilibrium position and the input position, $X - X_i$, is called the interpolation error. The interpolation error, when expressed as a function of X_i in a Fourier series over a period of one pitch, is usually dominated by the first and fourth harmonics.

Motor and Plotter Mechanism

For good line quality, interpolation error must be minimized, and this requires very accurate parts. However, low cost was one of the most important objectives for the 7225A Plotter. The attempt to achieve both low cost and good line quality made the design of the motor the major part of the 7225A project.

In the final design, the pole pieces are made of a stack of laminations. Each lamination is stamped with the proper pole spacings but without teeth, as shown in Fig. 3. The laminations are C1010 cold rolled steel. The permanent magnet is a rare earth

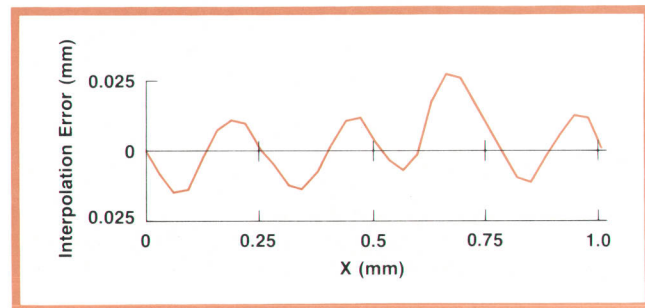


Fig. 5. Typical interpolation error of the linear step motor is less than 0.05 mm peak to peak.

Developing a Low-Cost Electrostatic Chart-Hold Table

by Alec J. Babiarz

The low cost objective of the new 7225A Plotter required new methods and processes to manufacture many standard assemblies. In the case of the chart-hold system the objective was to develop a low-cost version of the electrostatic table and derive a theoretical model for its operation.

The standard electrostatic chart hold was developed for flatbed plotters about fifteen years ago. Over the years questions have arisen about the table's operation that are not easily answered from a theoretical standpoint. For example, why do some types of paper hold to the table better than others? Why does paper hold to the table better in the humidity range of 40% to 50% than at 5% and not at all at 90%? Why will mylar sheets not hold very well? What characteristics of the table coating are pertinent to the table's operation? What is the optimum geometry for the grid pattern? How thick should the insulating layer below the grid pattern be? A better theoretical understanding of how the table works was necessary before these questions could be answered and the process of making the tables changed.

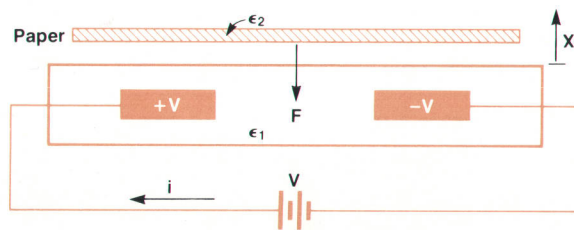


Fig. 1. The electrostatic table can be considered a capacitor to show that it exerts a force on the paper that is proportional to voltage squared.

Theory

A simple approach can be taken to show that a force can be derived from the electrostatic table. The table can be looked at as a capacitor (see Fig. 1). Let w = work, t = time, V = voltage, q = charge, c = capacitance, x = distance, and F = force. The power in the system can be written as:

$$\frac{dw}{dt} = Vi \quad (1)$$

where $i = \frac{dq}{dt}$ and $q = CV$. Therefore

$$i = C \frac{dV}{dt} + V \frac{dC}{dt} \quad (2)$$

Substituting (2) into (1) gives:

$$\frac{dw}{dt} = V \left[C \frac{dV}{dt} + V \frac{dC}{dt} \right]$$

Since the voltage source is a dc source, $dV/dt = 0$, so

$$dw = V^2 dC \quad (3)$$

We know that work is defined as

$$dw = Fdx \quad (4)$$

Substituting (4) into (3),

$$Fdx = V^2 dC.$$

Therefore

$$F = V^2 \frac{dC}{dx}$$

This simple model shows that the force developed by the table is a function of voltage squared. However it does not clearly indicate how the geometry or environment of the system affects the force. Therefore, a better model of the system was developed and a field analysis was done to obtain the force.

Fig. 2 shows the system model, boundary conditions, geometry, and coordinates with paper. The governing (Laplace) equations for solving the fields in the model and the stress exerted on the paper are as follows.

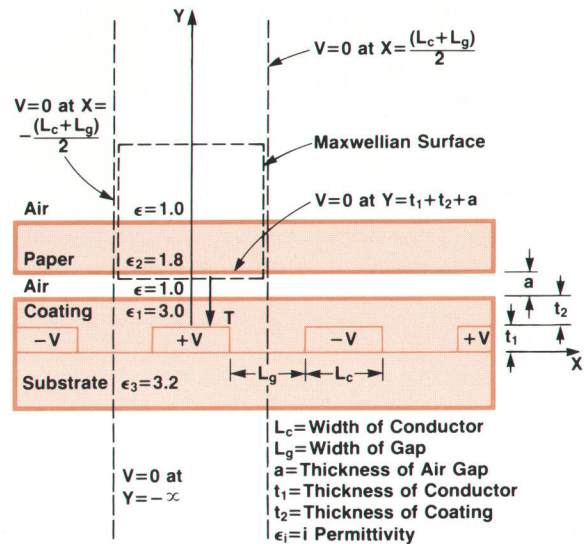


Fig. 2. A more complete model of the electrostatic table. T is the stress tensor. The Maxwellian surface chosen for the surface integral that defines the stress tensor is a cube, only one side of which can be seen in this two-dimensional view.

$$\begin{aligned}\nabla(\epsilon \nabla V) &= 0 \\ -\nabla V &= E \\ D &= \epsilon E\end{aligned}$$

where ϵ is permittivity, E is electric field strength, V is voltage, and D is the displacement vector, defined as shown.

Faraday-Maxwell field theory says that all forces are transmitted through one body to another in a continuous manner, much like the stress distribution in a body transmitting an applied load. Forces on a body in an electrostatic field come from forces on charges, forces from variations of permittivity at dielectric-vacuum interfaces, and effects of volume/density changes in the body. Maxwell's stress tensor equation describes the stress on an object enclosed by a Maxwellian surface in three-dimensional space in an electrostatic field.⁴ By taking a surface integral around the body one can find the triaxial forces on the body.

$$T_x = \epsilon_0 \left(\epsilon E_x^2 - \frac{E^2}{2} \left(\epsilon - \frac{d\epsilon}{d\sigma} \right) + \epsilon E_x E_y + \epsilon E_x E_z \right)$$

$$T_y = \epsilon_0 \left(\epsilon E_x E_y + \epsilon E_y^2 - \frac{E^2}{2} \left(\epsilon - \frac{d\epsilon}{d\sigma} \right) + E_y E_z \right)$$

$$T_z = \epsilon_0 \left(\epsilon E_x E_z + \epsilon E_y E_z + \epsilon E_z^2 - \frac{E^2}{2} \left(\epsilon - \frac{d\epsilon}{d\sigma} \right) \right)$$

where σ = density, ϵ = permittivity, ϵ_0 = permittivity of free space, and T is the stress tensor. By applying the boundary conditions, summing forces, and using the symmetry of the model, the stress tensor can be reduced to a simpler form.

$$T = \epsilon_0 \epsilon (E_y^2 - E_x^2/2)$$

or, since

$$E^2 = E_x^2 + E_y^2,$$

$$T = \epsilon_0 \epsilon (E_y^2 - E_x^2)$$

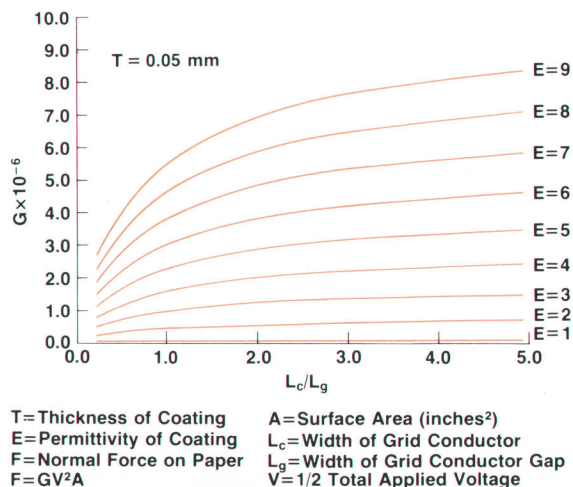


Fig. 3. Calculated theoretical force characteristics of the electrostatic table.

We now have the stress at the interface of the paper and the table coating that is purely dependent upon the E fields in the system. The E fields can be found by solving the Laplace equations (see above) for the model using the finite element method.^{1,2,3} Since the solution of the Laplace equations depends upon the applied boundary conditions, the permittivities of the materials, and the geometry of the model, this is a relatively complete steady-state model for the paper holddown force.

Results

Fig. 3 shows theoretical results for the force developed on the paper by a table. It was assumed that the potential field (V) went to zero in the paper surface and that the coating thickness was 0.002 in. The actual potential field in the paper depends on humidity and whether the "paper" is in fact a good dielectric like Mylar. Any potential greater than zero will lower the force curves.

Conclusions

It was found from this analysis that the table force could be increased by:

1. Increasing coating permittivity
2. Decreasing coating thickness
3. Increasing insulating substrate thickness to at least 0.10 in from a ground plane
4. Making $L_c/L_g > 2$
5. Maximizing applied voltage.

It was also found that the grid conductor could be thin (10 μ in) and of relatively high resistance (200 Ω) without affecting the force. This information led to the use of a molded plastic table with electroless copper plated grid conductors and a silkscreened paint surface coating. This new process cut the manufacturing cost of the table by a factor greater than two.

References

1. H.C. Martin and G.F. Carey, "Introduction to Finite Element Analysis, Theory and Application," McGraw Hill Book Co., New York, 1973.
2. K.C. Rokeby, H.R. Evans, D.W. Griffiths, and D.A. Nethercot, "The Finite Element Method, A Basic Introduction," A Halsted Press Book, John Wiley & Sons, New York, 1975.
3. B. Nath, "Fundamentals of Finite Elements for Engineers," The Athlone Press of the University of London, 1974.
4. R. Becker, "Electromagnetic Fields and Interactions, Electromagnetic Theory and Relativity," Vol. 1, Blaisdell Publishing Co., New York, 1964.

Alec J. Babiarz



Born in Hartford, Connecticut, Alec Babiarz is a 1972 BSE graduate of Arizona State University and a 1973 MSME graduate of Stanford University. Alec was responsible for the thermal writing system for the 7130A Strip Chart Recorder. For the 7225A Plotter, he designed the electrostatic table and worked on the design of the pen lift. He is also named inventor on a patent application for electrostatic table manufacture. A resident of Leucadia, California, Alec is single and keeps active in his leisure time by cross-country skiing and playing bridge.

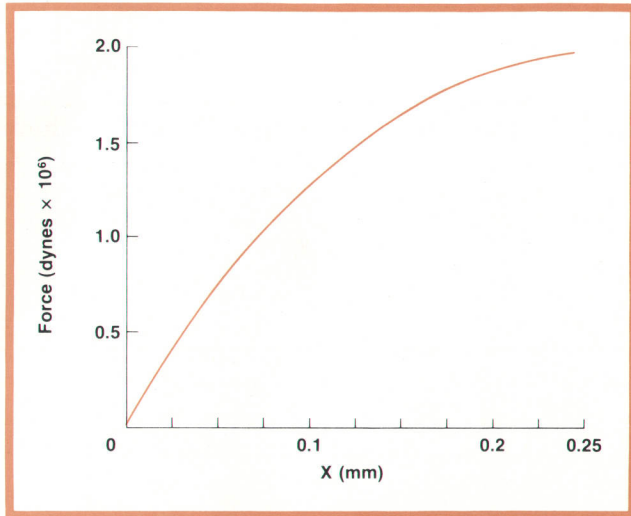


Fig. 6. Force versus displacement for the X motor.

cobalt magnet that has a magnetic energy product of 16×10^{15} oersteds. The laminations are stacked to the required height in a fixture and then wound with the proper number of turns of wire. The complete stack with the permanent magnet is inserted into the housing of the mover and potted with epoxy as shown in Fig. 4.

After potting, the pole pieces are machined and the teeth of the mover are cut in a single pass with a cutter that is accurate within ± 0.005 mm. The final pitch is

1.016 ± 0.007 mm, tooth width is 0.457 ± 0.007 mm, and tooth length is 0.305 ± 0.051 mm.

Two side plates with pre-assembled support and guide bearings are bolted onto the mover housing in a gapping fixture. Any assembled mover can be placed on any stator to complete a motor. The motor air gap is maintained by the support bearings at 0.0508 ± 0.0102 mm. The motor made under these conditions typically has a peak-to-peak interpolation error of 0.050 mm (0.002 inch), as shown in Fig. 5. Fig. 6 shows the force-versus-displacement curve for the X motor.

The mover is guided by three preloaded guiding bearings. The Y-mover rides on the Y stator, which is driven by the X-mover over the X-stator (Fig. 7). The pen assembly is mounted on the Y-mover. This completes the X-Y mechanism without using pulleys, cable, and gears.

Stator Construction

The stators for the linear motors presented several interesting manufacturing problems. The teeth mating with the mover pole pieces have a pitch of 1.016 mm (see Fig. 2). An absolute position accuracy of ± 0.0050 mm non-accumulating over 37 pitches was needed so that the motor could interpolate (move stepwise through the pitch) with the desired accuracy of 0.050 mm. The geometric configuration and the tooth width and depth have been shown to contribute to this interpolation accuracy. Besides providing the

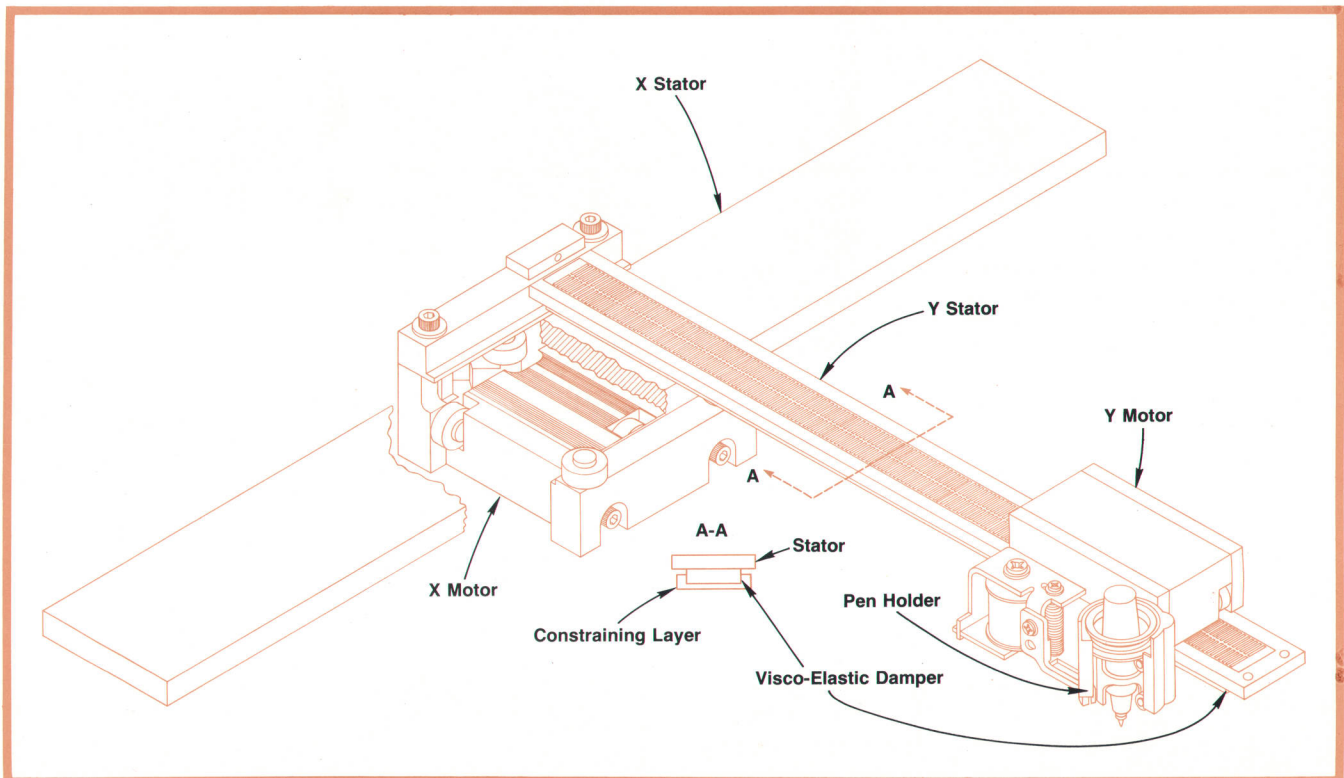


Fig. 7. 7225A Plotter X-Y mechanism.

magnetic path for the linear motors, the stators also support and guide the motion of the motors. This calls for a very flat, wear-resistant surface that can endure 100 miles of plotting and adds minimal reluctance to the magnetic circuit. The positioning of the guide bearings and the stepping motion of the motor produce a position-dependent variable cyclic loading. This loading develops a maximum shear stress of $1.2 \times 10^8 \text{ N/m}^2$ (18,000 psi) at a location 0.023 mm below the surface. The fatigue life of the bearing surface is well over an order of magnitude larger than the required 2×10^6 cycles.

To achieve the objectives of low cost, high wear resistance, and a good magnetic path, the stators are assembled from two separate parts, a laminate and a magnetically soft blank (Fig. 1). The laminate is chemically machined from 0.25-mm annealed low-carbon steel. The chemical machining process can repeatedly produce high-position-accuracy parts from a glass master. This provides consistent and repeatable pitch placement of $\pm 0.005 \text{ mm}$. Since the laminate is machined through the material, the etch depth is held to the material thickness tolerance, $\pm 0.008 \text{ mm}$. The local variations of the tooth width are within $\pm 0.05 \text{ mm}$ and average out over the area of the pole pieces. This laminate provides the stepping geometry of the stator.

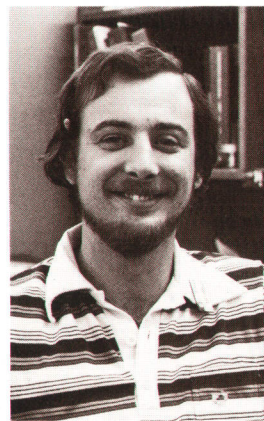
The blanks are also low-carbon steel as required for the magnetic path and are double-disc ground flat and plated with $0.010 \pm 0.003 \text{ mm}$ of hard chrome ($R_C=70$). This produces a flat, wear-resistant surface and a chrome-steel interface well above the maximum shear stress. A thermosetting adhesive is applied to the laminates and they are heated together with blanks under $1.4 \times 10^6 \text{ N/m}^2$ (200 psi) pressure. This process is controlled such that the adhesive bond line thickness is 0.0013 mm or less. Once assembled, the stators are completely interchangeable with any motor. From bearing surface to the top of the teeth the stators measure $0.25 \pm 0.009 \text{ mm}$. The motors are pre-loaded and set for a bearing-to-teeth gap of $0.30 \pm 0.0013 \text{ mm}$, so the magnetic air gap is held to $0.05 \pm 0.010 \text{ mm}$.

The motor ball bearings have been extensively tested and analyzed. The loading on the bearings is cyclic and calculations show a B_{10} life* exceeding 16×10^6 revolutions or 1000 miles of linear travel. The ball bearings are ABEC Class 3 self-aligning bearings. Their radial play is adjusted to reduce perpendicularity tolerances with respect to the stator, thus reducing manufacturing cost.

The Y-axis stator is cantilevered from the X motor (see Fig. 7). The fundamental transverse resonance is at 60 Hz, and with the driving force of the Y-motor,

the undamped peak amplitude was sufficient to cause the pen to leave the plotting surface during writing. To prevent this, the stator was damped by a method of constrained-layer damping. A beam in bending has a parabolic shear flow distribution through the thickness with maximum shear at the neutral axis of bending. Placing a high-loss material such as cured rubber at this point causes some of the energy to be absorbed through shear hysteresis during vibration. To gain the highest efficiency, a constraining layer is used to place the damping material as close to the neutral axis as possible (see Fig. 7). Given the space constraint, an optimal sandwich can be determined. The system was modeled using an aluminum-rubber-steel composite beam, and by matching moments of inertia and moduli of elasticity (rubber having a complex shear modulus that can be related to the loss factor of a visco-elastic material), an optimum configuration was determined. The damping efficiency depends upon temperature and frequency of vibration, but remains fairly constant over the plotter's operating

Robert L. Ciardella



Born in San Francisco, California, Bob Ciardella received his BSME degree and his BS degree in material science in 1974 and his MSME degree in 1975 from the University of California at Berkeley. Bob has been an HP employee since 1976 and designed the linear step motors and pen lift for the 7225A Plotter. He is also named inventor on a patent for a superconductor manufacturing process. An Encinitas, California, resident, Bob is single, enjoys skiing, volleyball, and holds a brown belt in karate.

Lung-Wen Tsai



A native Taiwanese, Lung-Wen Tsai received his BSME degree from the National Taiwan University in 1967, his MSME degree from the State University of New York at Buffalo in 1970, and his PhDME from Stanford University in 1973. Tsai, as his colleagues call him, designed the linear step motors for the 7225A Plotter and contributed to the design of the 3968A Instrumentation Tape Recorder. Married, with a son and a daughter, Tsai has recently left HP to join General Motors Research Laboratories in Warren, Michigan. Gardening, fishing, and playing bridge keep Tsai busy in his off-hours.

* B_{10} life, a standard measure of bearing life, is defined in all standard bearing handbooks. Briefly stated, it is the point at which 10% of the bearings have failed.

range at approximately 4% critical damping. Damping in this manner added little extra weight to the moving mass and provided enough reduction in the resonant amplitude to achieve the desired writing quality. 

References

1. W.E. Hinds, "The Sawyer Linear Motor," Proceedings of Second Annual Symposium on IMCSD, Department of

Electrical Engineering, University of Illinois, Urbana, Illinois, April 1973, pp. W1-W10.

2. H.D. Chai, "Permeance Model and Reluctance Force Between Toothed Structures," Proceedings of Second Annual Symposium on IMCSD, Department of Electrical Engineering, University of Illinois, Urbana, Illinois, April 1973.

3. A.L. Jones, "Permeance Model and Reluctance Force Between Toothed Structures," Proceedings of Fifth Annual Symposium on IMCSD, Department of Electrical Engineering, University of Illinois, Urbana, Illinois, May 1976.

Simple, Efficient Electronics for a Low-Cost X-Y Plotter

by William G. Royce and Peter Chu

A PRINCIPAL GOAL of the Model 7225A Plotter development was to minimize both initial and maintenance costs without sacrificing operating features. This, in combination with the relatively small size of the plotter, imposes severe constraints on the electrical design. An additional requirement, compliance with worldwide safety and EMI codes, has a great effect upon primary wiring, components, and EMI filtering. The single most effective technique for achieving all of these goals is to minimize power.

Switching drivers, regulators, and converters immediately come to mind as means for achieving efficient conversion of line power to useful loads. However, a switching converter is not a practical way to obtain secondary dc power for this application. It is complex, costly to build and service, requires bulky and expensive EMI filters, and is not justified for small load power, while a power transformer, especially if high leakage inductance can be tolerated, is very helpful in meeting safety and EMI requirements. Power needs of the ± 12 volt supplies are also small and are readily satisfied with three-terminal regulators. The motors, on the other hand, are well-suited to switching drivers, because they exhibit a high ratio of dynamic to static voltage drops at high current. Of course, switching drivers are more complex and costly than linears, but the improved efficiency sharply drops power transformer size and cost and reduces cooling needs. These benefits are particularly needed in a small unit. Similarly, the logic supply power is great enough to justify the added complexity of a switching regulator.

Motor Drivers

Sine and cosine current drivers are required for each motor. To minimize position interpolation error and dynamic problems, these drivers must have low dc offset and low harmonic distortion, and must be well-matched in gain and phase. A switching driver with current feedback, operating at a switching frequency much higher than the motor-drive frequency, efficiently provides the high output power needed, but lacks dc offset control and gain accuracy. These are most easily provided by adding an integrator stage

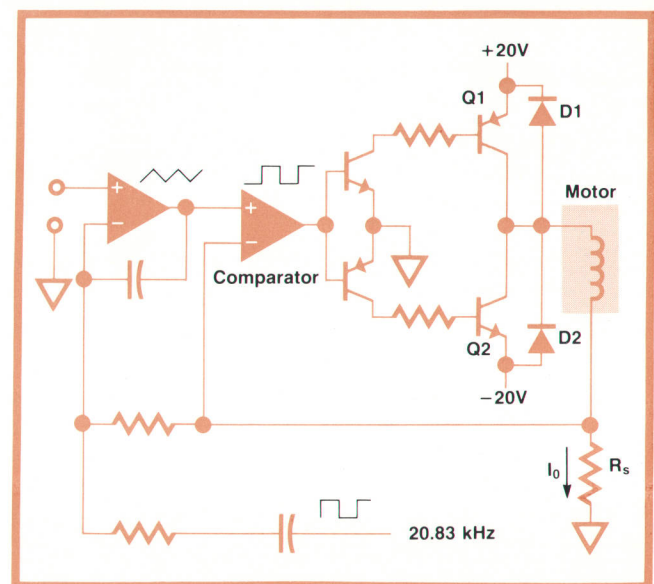


Fig. 1. Motor drivers have low dc offset and low harmonic distortion.

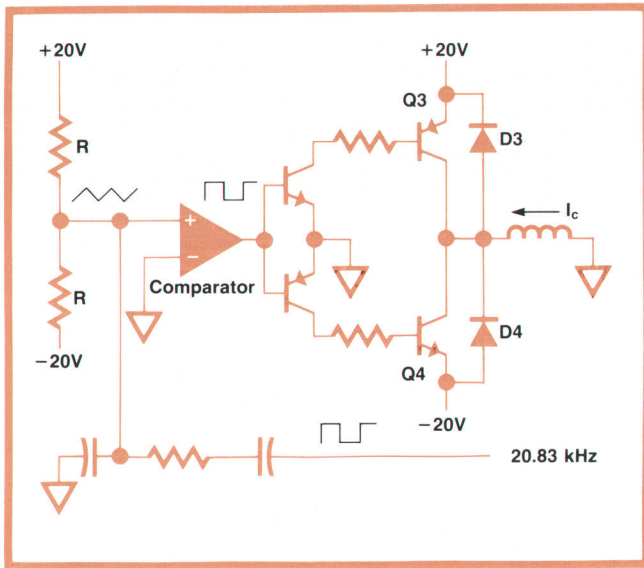


Fig. 2. Voltage balancer restores balance when the motor drivers draw current from one power supply and pump part of it to the other.

ahead of the switchers and employing overall feedback. This combination has very high loop gain for dc and the low motor drive frequencies of interest (up to 250 Hz), along with low dc offset and high input impedance.

A controlled-amplitude triangular-wave forcing function must be provided at the input to each switching driver stage. This signal controls loop gain and prevents self-oscillation. The four drivers must also be operated at the same switching frequency to avoid low-level but audible intermodulation products. Both of these needs are satisfied by a common 20.83-kHz square wave applied to each system. The square wave drives the integrator stage to obtain the triangular wave. Fig. 1 is a simplified diagram of the driver amplifiers.

Voltage Balancer

There are two ways to obtain the bipolar currents for the motor. One is to use a single power supply with a bridge-type output stage. This circuit arrangement is relatively complex, especially if precision current control is required. The alternative is to use two supplies and a bipolar drive, as in the 7225A. The circuit is simpler and feedback is straightforward, but there is a potential problem. With a dc current in the motor winding, a current is forced into one supply. For example, in Fig. 1, if I_0 , the average motor current, is positive as shown, current will be drawn from the +20V supply through Q1 when the comparator output is positive. When the comparator again switches, Q1 is turned off and Q2 is turned on. Because of the inductance of the motor windings, current I_0 continues to flow in the same direction, mostly

through D2 and partly through Q2. Thus the energy from the +20V supply that is stored in the motor inductance during the positive part of the cycle causes the motor to act as a current source charging the -20V supply during the negative part of the cycle. If the current loading of the -20-volt supply does not at least equal the pumping current, the supply voltage rises, eventually back-biasing the rectifier diodes. With four motor drivers, there is a high probability that one of the supplies will be pumped to a high voltage unless something else is done.

The simplest cure is to load each supply sufficiently to exceed the maximum current pumped in. This is grossly inefficient and therefore unacceptable. We have chosen to add another driver, similar to the motor drivers but with a low-loss inductor load. Input to this driver is the mean value of the 20-volt supplies, as shown in Fig. 2. Suppose, as above, that excess current is being pumped by the motor drivers into the -20-volt supply. The resulting voltage unbalance causes this driver to output a current I_c in the direction shown. This current is taken from the -20-volt supply during the negative part of the cycle and continues to flow in the same direction through D3 during the positive part of the cycle. Thus when the motor drivers draw current from one supply and pump part of it to the other, this driver acts oppositely to restore voltage balance.

Autogrip Supply

The high-voltage supply for the autogrip electrostatic platen presents a challenge for low-cost systems. A dc voltage differential of 800 to 1000 volts at negligible current is required to hold the paper well. In the past this has been obtained using a high-voltage winding on the main power transformer or a separate

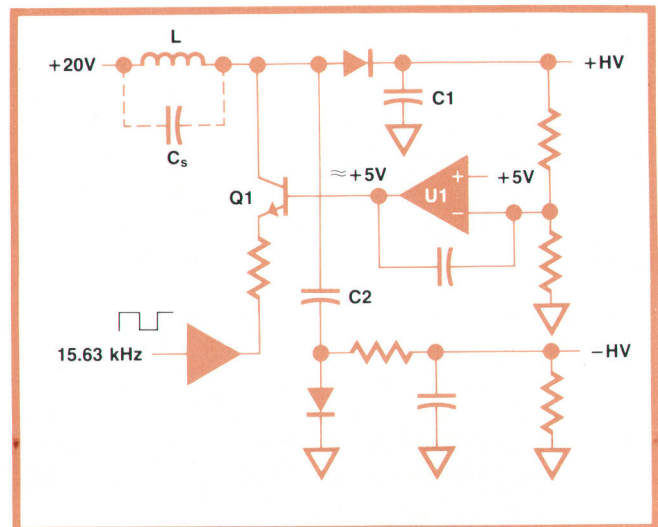


Fig. 3. Autogrip supply meets requirements for a high voltage differential, safety, and low cost.

transformer along with a voltage-doubler rectifier. On-off control was via a switch in series with the transformer winding. With more recent product safety requirements, the cost of this approach has risen sharply. For example, on-off control is best provided now by a low-level switch and driver controlling an approved relay.

The 7225A uses a ringing circuit to obtain a train of high-voltage pulses. In Fig.3, the resonant circuit consists of a small molded inductor, L, and the lumped stray capacitances, C_s . A TTL buffer forces current into the emitter of Q1 and causes the current to increase in L. At the end of this half-cycle, the buffer output goes high and Q1 abruptly shuts off. This leaves the L-C circuit with initial current in the inductor. The current in L continues to flow, charging C_s until its voltage equals that of C1 and C2. At this point the remaining current, which has been decreasing cosinusoidally, charges C1 and C2 until the coil current is zero. Now the coil voltage falls again toward zero driven by the charge on C_s . Ignoring losses, loading of the rectifiers, and semiconductor breakdowns, the peak voltage is given by:

$$V_p = I_L \sqrt{L/C_s}$$

where I_L is the initial current in L. Typical values of $I_L = .04$ A, $L = .01$ H, and $C_s = 25$ pF give $V_p = 800$ volts. Typical RF losses reduce this to approximately 700 volts. Rectifier system loading drops this to a lower value, but it is still high enough to exceed com-

ponent ratings. In keeping with a policy of no electrical adjustments in spite of temperature and component variations, a regulating circuit was added. The magnitude of I_L is most easily controlled by the base voltage of Q1. U1 compares the positive output voltage to the +5-volt supply and adjusts the base voltage of Q1 as needed. On-off control is obtained by gating the 15.63-kHz input to the buffer.

5-Volt Logic Supply

The +5-volt load current is substantial in a digital system like the 7225A. To meet the goal of efficiency, a switching regulator was chosen, similar in design to a motor driver. It employs a switching power stage preceded by an integrator that also uses the same 20.83-kHz square-wave drive to generate the triangular wave. The high-Q L-C filter needed to achieve low output ripple imposes a difficult loop stability problem. Such a filter has complex poles very close to the imaginary axis. The filter poles are included within the local loop around the output switcher, raising their Q even higher. The problem was solved by damping the filter directly with a capacitor and resistor, then adding a step in the integrator's response.

The regulator operates from the +20-volt supply, achieving a nearly constant efficiency of 75 percent. This is much better than a linear regulator would have achieved, given the poor regulation of the power transformer necessitated by other design considerations. Cost of the two approaches is virtually the same.

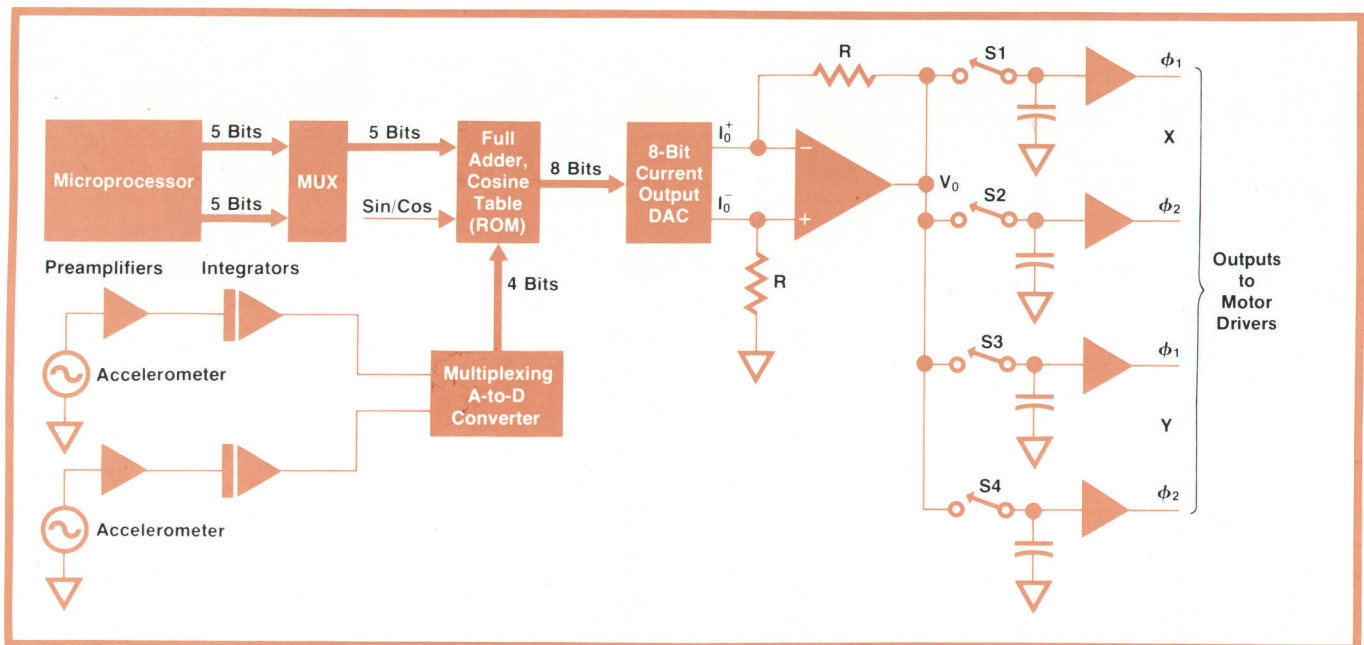


Fig. 4. Microstep control system supplies each motor driver with two sinusoidal signals 90° out of phase. The switches are closed individually for 8 μs, charging the corresponding capacitors to V_o . The delay between the closing of S1 and the closing of S2 is 16 μs, equivalent to 1.44° at the highest motor speed.

Microstep Control System

Each of the two linear motors (X and Y) is driven by two sinusoidal waveform signals, their phases separated by 90°. To reduce the number of electronic components, the four signals are generated one at a time. High-speed multiplexing and demultiplexing (i.e., fast relative to the maximum drive frequency) introduces little phase error even at the highest moving speed. In the circuit of Fig. 4, switches S1, S2, S3 and S4 strobe the digital-to-analog converter (DAC) output in specific time windows. These samples, in general, can be expressed as:

$$f(t) = \sum_{n=0}^N \delta(t-n\Delta T) \left\{ -\cos \left[(S+M+8I)\Delta\theta + \frac{\Delta\theta}{2} \right] + E(n) \right\}$$

where:

$\Delta T = 128 \mu s$, the sampling time interval

$0 \leq S \leq 31$, the microstep number generated by the microprocessor according to the positioning algorithm

$0 \leq M \leq 15$, the feedback microstep number derived from the digitized accelerometer output signal

$I = \begin{cases} 0, & \text{sine function} \\ 1, & \text{cosine function} \end{cases}$

$\Delta\theta$ is the incremental phase unit

$E(n)$ is an error term, explained below.

The sum $(S+M+8I)$ is applied as an address input to a 32×8 ROM programmed as a cosine look-up table starting at 5.6°. $E(n)$ is the error associated with the

n th step and includes the truncation error of the eight-bit output, tolerances of components, and dc offsets in the DAC and switches.

The cosine wave is divided into 32 steps, making $\Delta\theta = 11.25^\circ$. Eight steps represent a phase change of 90°. In the absence of an acceleration signal, M has the value of 8. For $S = 0$, $M = 8$, and $I = 1$, $-\cos(185.6^\circ) = \cos(5.6^\circ)$. Of course, the designations "sine" and "cosine" indicate only a 90° phase difference and have no other meaning.

The error term $E(n)$, plus the dc offset from the sample-and-hold and driver amplifier directly affects the motor's interpolation error. The total dc offset and harmonic distortion of the driving current has been designed such that the interpolation error is less than 0.05 mm (peak to peak).

To eliminate any dc offset adjustment for the unsigned DAC, a differential output DAC is used. When its input is all zeros, $I_0^- = \text{full scale}$ and $I_0^+ = 0$, and when the DAC input is all ones, $I_0^- = 0$ and $I_0^+ = \text{full scale}$. Thus the dc offset depends only on the DAC's output current symmetry and other component tolerances, such as resistor value matching and operational amplifier offset.

Since there are only 15 different quantized levels (peak to peak), the half points, $\sin 0^\circ$ and $\cos 90^\circ$, do not exist in the ROM.

The accelerometer signals are amplified, integrated, and then digitized by the multiplexing analog-to-digital converter (Fig. 5a). The converter is a simple one, using the dual-slope method. It has a four-bit "offset binary" data output. It operates con-

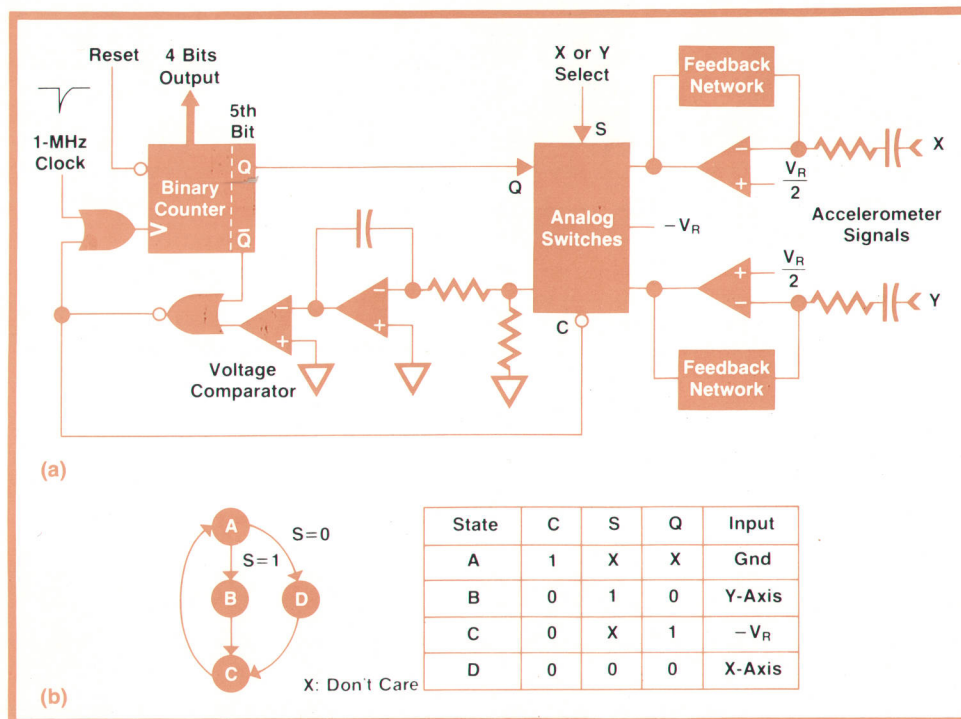


Fig. 5. (a) Multiplexing analog-to-digital converter amplifies, integrates, and digitizes the accelerometer signals. The reset pulse starts the conversion, setting the counter output to zero. The fifth bit changes the integrator input to $-V_R$ to discharge the capacitor. (b) State diagram for analog switch control.

tinuously from the time power is turned on. Thus, even when the plotter is in stand-by (no motion) mode, any mechanical vibration that causes an accelerometer response will result in a counteracting drive to the motors.

Total conversion time for a full-scale signal is $32 \mu\text{s}$. The accelerometer's ac signal, having been filtered, is biased at $V_R/2$ and limited to less than V_R . Thus it appears at the input of the dual-slope integrator as a positive voltage. The fifth bit of the binary counter helps in steering the inputs between $-V_R$ and the accelerometers.

It is easy to see how the multiplexer works from the

state diagram, Fig. 5b. In state A, no current flows into the integrator and the last converted data is left in the counter. In state B, the Y accelerometer signal input is on for $16 \mu\text{s}$. In state C, only $-V_R$ is on, discharging the capacitor until the voltage reaches its starting point. In state D, the X accelerometer signal input is on for $16 \mu\text{s}$.

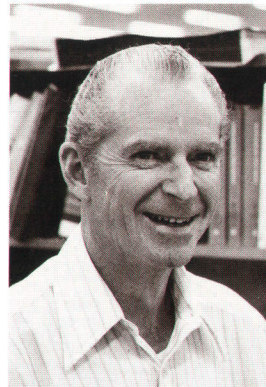
The reset pulse occurs every $64 \mu\text{s}$ to reset the counter to zero, initializing a new conversion. This ADC has good high-frequency noise rejection, and its noise immunity is $\pm 1/2$ LSB (least significant bit) for low-frequency noise. 



Peter Chu

Born in Kwei-Chow, China, Peter Chu is a 1966 BEE graduate of Georgia Institute of Technology and a 1968 MSEE graduate of Colorado State University. Peter joined HP's Loveland Instrument Division in 1966, then transferred to San Diego Division in 1973 where he designed the digital/analog converters for the 7225A Plotter and is now designing 7225A personality modules. He is also named inventor on a patent relating to pulse code modulation. A resident of Poway, California,

California, Peter is married and spends much of his leisure time woodworking, skiing and flying Cessna 150 airplanes.



William G. Royce

Bill Royce received his BS degree in 1949 from San Diego State College and his MSEE degree in 1972 from Colorado State University. An HP San Diego Division employee since 1973, Bill was project leader on the 3968A Tape Recorder and electrical designer for the 7225A Plotter. Bill is the author of several published articles on data amplifiers and grounding for dc instrumentation systems and is named inventor on two patents relating to recording. Born in Spokane, Washington, Bill is married

with four grown children and lives in San Diego, California. Reading, gourmet dining, and listening to classical music keep Bill busy in his leisure hours.

A Closed-Loop System for Smoothing and Matching Step Motor Responses

by Philip P. Maiorca and Norman H. MacNeil

TRADITIONALLY, STEP MOTORS are thought of as open-loop position devices, that is, an input signal results in a position output. In the case of an X-Y plotter, where straight-line accuracy is dependent upon smooth and matched responses on the two axes, underdamping can cause problems in step-motor systems.

The inherent Q of a step motor is usually greater than 5, so transient responses are not smooth. Also, system responses near or at resonant frequency often have gains greater than 5, a problem if perturbations

are generated that have frequencies in this region. Such perturbations do arise in step motors because of lack of harmonic purity in both the reluctance of the stator and the motor drive currents. The frequency of these perturbations is a function of the instantaneous velocity of the motor. Thus, at particular angles, frequencies can be generated that fall within the passband of the step motor, giving rise to "wiggles" that can exceed 0.5 mm—the so-called "slew" (constant velocity) resonances.

For these reasons, a scheme for damping the motor

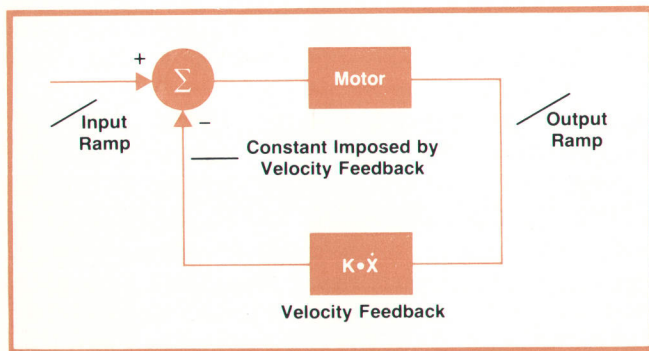


Fig. 1. For a second-order system like the linear step-motor, velocity feedback is the most desirable type. However, dc velocity feedback results in increased static lag during slew or acceleration. For example, with a ramp input, the output is a ramp, and a constant value is fed back to the summing junction, imposing more steady-state lag. For this reason, ac velocity feedback is used.

is necessary. Damping can be achieved either mechanically or electronically. For a linear step motor, a mechanical damper proves more costly and less reliable than an electronic feedback loop. Therefore, the position control servo in the 7225A Plotter is a closed-loop system.

Velocity Feedback

For a spring-mass system (2nd order) velocity feedback is the only inherently stable feedback type. If position feedback is used, there is a potential stability problem at the high gain-crossover frequencies. If acceleration (or higher-order derivative) feedback is used, a like problem exists at low frequency. The basic useful properties of velocity feedback are:

1. Does not alter open-loop resonant frequency.
2. Determines closed-loop Q of the system virtually independent of the open-loop Q.
3. Limits phase margin at gain crossover (high or low frequency) to $\pm 90^\circ$.

These properties hold for pure dc velocity feedback. However, this type of feedback is difficult to achieve, since it must be derived from either a differentiation of position, which has noise problems at low frequency, or from a frequency detecting encoder, which suffers sample rate problems at low frequency. Dc velocity feedback is also undesirable because of the static lags that are developed during slew or acceleration, making axis matching more difficult (see Fig. 1). Since velocity feedback is necessary only at resonance, ac velocity feedback serves the purpose without increased steady state lags and sacrifices little of the advantages mentioned above.

In view of these considerations, a device was needed to deliver ac velocity feedback without any attachment to a slidewire, pulley, or other encumbering device, since the goal of the project was to eliminate pulleys, slidewires, encoders, etc. Because the

step motor is linear instead of rotary, an inertial sensing device was necessary. The choice was a bimorphic piezoelectric beam that senses acceleration and transduces it into an electrical signal. This acceleration signal is integrated to produce the desired ac velocity feedback. The design of this accelerometer is described later in this article.

Velocity feedback is implemented by sensing the acceleration with the bimorphic accelerometer, integrating the output (resulting in ac velocity feedback), performing an analog-to-digital conversion, and finally digitally taking the difference of the input microstep and this digital representation of ac velocity (see Fig. 2). The resolution is 0.03 mm and sufficient damping is achieved to keep the amplification of perturbations in the passband to less than 1 dB. The bimorphic accelerometer has a Q on the order of 50, and although its resonance is at a rather high frequency (7.5-8.5 kHz), it can create a problem at high-frequency gain crossover. To alleviate this problem, the sample rate of the A-to-D converter was set to 7.8 kHz, which achieves a 20-db attenuation of the beam resonance for the primary (dc) spectrum (see Fig. 3).

X-Motor Accelerometer Placement

The next question was where to place the accelerometer to achieve adequate damping of the resonances. In the case of the X motor, this was not a trivial problem. Since the X axis carries the Y axis, a cantilever is added to the mass of the X axis. Since forces are applied to the X motor away from the center of mass of the system, a moment is also applied to the system and a second resonant frequency is obtained rotationally. This frequency is determined by the rotational inertia and the torsional spring constant formed by the guiding bearings. Thus, the motion equation for inputs to the X motor has two primary coupled resonant frequencies, one translational and one rotational. For a system of this type, it can be shown that placement of the transducer must be on the X-motor side of the center of mass.

The magnetic flux that produces the force to move the motor in the horizontal direction also produces normal forces. As the various pole pieces energize, the normal forces applied change position and thus generate moments directed along the Y axis. This gives rise to a rocking motion that is restricted by the support bearings. Again, another resonant frequency results that is determined by the rotational inertia and the torsional springs formed by the support bearings. The X-motor transducer senses motion principally in the X direction, but since rotational modes exist that give rise to angular velocities in the Y and Z axes, the transducer senses these motions also, and these resonances appear inside the loop. In addition, since there is no symmetry axis for the total mass system, cross-

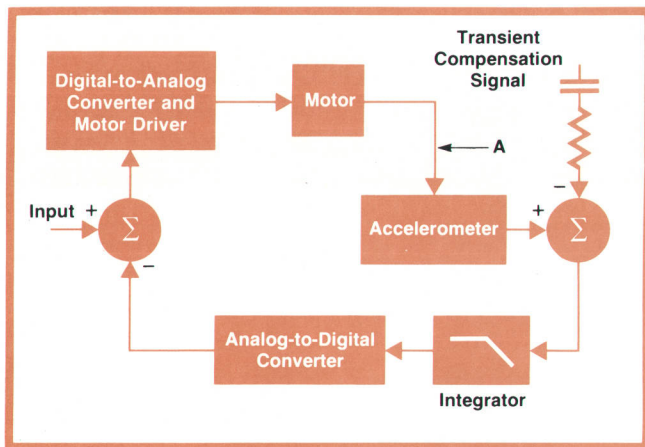


Fig. 2. Ac velocity feedback is derived by integrating the output of an accelerometer mounted on each motor. The summing junction then takes the difference between the digital microstep input and the digitized integrator output. During acceleration the signal at point A is a rounded square wave. A square wave out of phase with this signal is added ahead of the integrator to minimize the transient effects of acceleration.

moments of inertia exist that couple all modes of rotational vibration to each other. These additional modes are of a higher frequency and of rather high Q (>10). This can be quite disconcerting for high-frequency stability.

A careful study was made of where to place the transducer on the X motor to minimize the additional summing effect of these higher-frequency resonances on the total open-loop response. To this end, extensive use was made of the HP 5451B Fourier Analyzer. Laborious probing was done with an accelerometer at various points on the X motor to obtain an overall profile in frequency that would maximize sensing of the primary resonances and minimize sensing of the higher-frequency resonances.

Matching Axis Responses

Once the servo was made stable, other considerations for line quality were considered. One problem of primary importance to straight-line integrity is matching of axis responses, and the key to these responses is lag, defined simply as the difference between the motor input and the output position. The basic problem reduces to matching in time the lags developed by both axes.

The determining factors for lag response time are the resonant frequency of the system (force to mass ratio) and the Q of the system.

The feedback makes the Q of each axis inversely proportional to the resonant frequency. This helps slow down the faster responding axis (because of its higher resonant frequency) and thus tends to match the responses.

Since the transducer is a piezoelectric device, it

does not sense dc acceleration, so it ac-couples the acceleration. This is desirable because no static lags are developed during acceleration. However, during acceleration a transient derived from the accelerometer-integrator is injected into the summing junction, yielding an increase in apparent lag. These increased lags in themselves are not harmful, since both axes are subject to the same transients. However, two undesirable effects result from these transients. One is that the dynamic range of the A-to-D converter can be exceeded, resulting in saturation and thus loss of damping. Second, during deceleration these lags become leads, which can result in overshoot on lines being drawn. This makes it necessary to cancel these transients to minimize the total lags of the axes. This cancellation is achieved by summing a square wave out of phase with the output of the transducer during acceleration and deceleration (see Fig. 2). Since the force-to-mass ratios of the two motors are not exactly matched during acceleration, more lag occurs on the X axis, so a larger compensation signal is summed into the X axis. Overcompensation of the X axis helps preserve line quality when short lines are drawn, such as when annotating or plotting graphs.

The 7225A Plotter, using this feedback scheme, will typically exhibit less than 0.13 mm peak-to-peak deviation from a straight line for all lines. This includes motor matching, transients, and slew resonances.

Noise Reduction

Audible noise is always an objectionable property of instruments that move mass. In the 7225A Plotter,

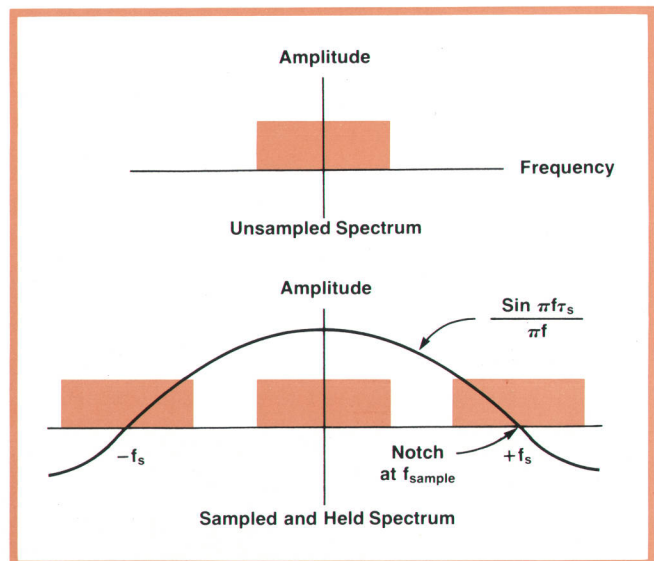


Fig. 3. The analog-to-digital converter has a sinc/x transfer function. 20-dB attenuation of the accelerometer resonance is obtained by making the sampling frequency approximately equal to the accelerometer resonance frequency.

the changing magnetic fields in the stator produce stresses that result in bending moments in the stator, which in turn move the arm and cause noise. This effect can be quite undesirable during acceleration when frequencies of the drive currents are low. To aid in the reduction of noise, the motor currents are low-pass filtered at 700 Hz. This reduces noise in the frequency range from 1 kHz to 4 kHz where the human ear is most sensitive. Since this single-pole filter is inside the feedback loop, it reduces the phase margin at high gain crossover. This effect of the filter is compensated for by a zero placed in the integrator at 700 Hz.

Accelerometer Design

The accelerometer used to sense motor movement is a relatively small, low-cost hybrid. Its dimensions are 19.3×16.2×3.5 millimeters, and its mass is two grams.

Since the accelerometer signal uses the same cable as the switched motor drive currents, the accelerometer signal has to be large and have low source impedance. An amplifier was included in the accelerometer package to achieve this.

The circuit configuration and component values were arrived at by a series of trade-offs. The input impedance is dictated by the servo design requirements, the beam size, and the required frequency response. The feedback network is split into a direct current section (adjustable in gain from 3.9 to 7.8) and an alternating current section (fixed at a gain of 21.5) to minimize the zero offset while also minimizing the sizes of the coupling capacitor and its associated resistor.

Since a given accelerometer sensitivity is required, five binary weighted resistors are provided for sensitivity adjustment.

The accelerometer is constructed on a thick-film ceramic substrate containing 11 thick-film resistors ranging in value from 15 kilohms to 220 megohms (Fig. 4). A capacitor is also formed in the thick film by using a glass dielectric and crossing conductors. An

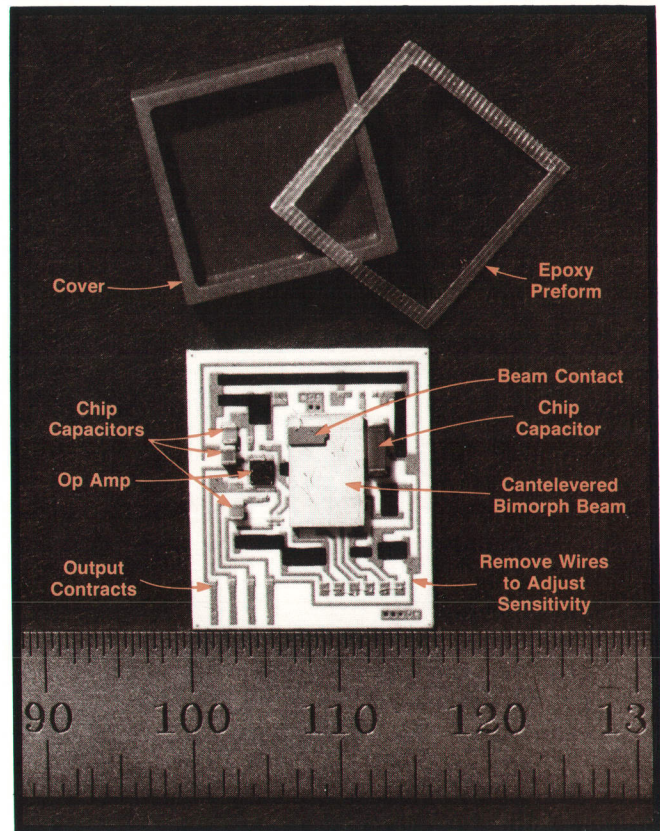


Fig. 4. Bimorph beam accelerometer senses motor movements.

operational amplifier chip, four chip capacitors, and a cantilevered piezo-electric bimorph beam are fastened to the substrate, mechanically and electrically, by a silver-filled epoxy. Gold wire bonding is used to make the remaining circuit connections. The finished hybrid is protected by a ceramic cover sealed by epoxy after filling with dry nitrogen.

In production, the accelerometer is built six-up on scribed substrates. All assembly and leak testing are done before separation. After separation and aging the unit is tested and its sensitivity adjusted. The external sensitivity trim wirebonds are then covered

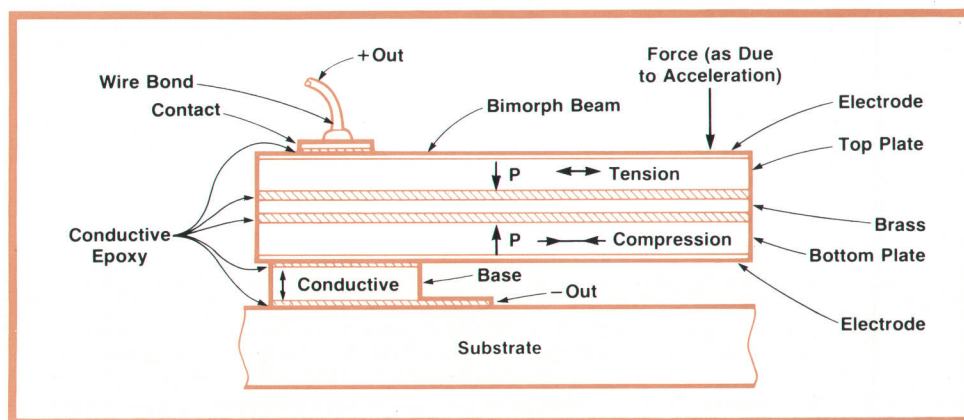


Fig. 5. Construction and mounting of the bimorph beam acceleration sensor.

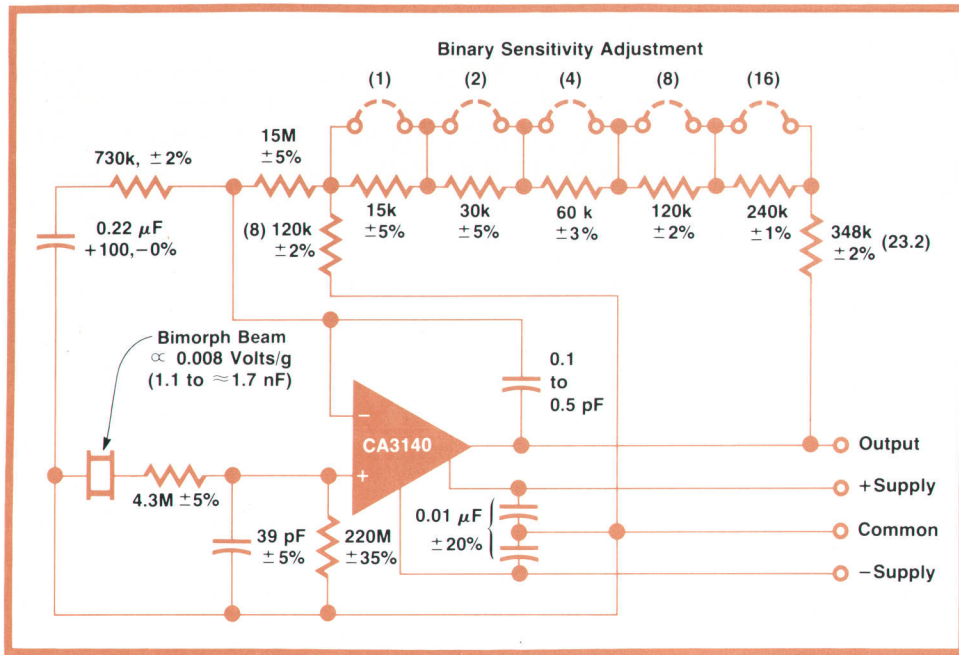


Fig. 6. Accelerometer schematic.

with epoxy and the unit is placed in protective packaging.

The acceleration sensor beam is a sandwich of two oppositely poled lead-zirconate-titanate piezoelectric ceramic plates with a center brass piece (Fig. 5). Bending the beam produces tension in one plate and compression in the other, thus generating an electrical signal in each plate. The sum of these signals appears between the top and bottom electrode surfaces. The mass of the beam, when subjected to acceleration, produces the force necessary to bend the beam. When mounted with a five-millimeter cantilevered section, it produces approximately eight millivolts per standard gravity of acceleration and deflects, for the same acceleration, 2×10^{-8} meters at the end. The capacitance of the beam is, nominally, 1.5×10^{-9} farads.

The operational amplifier chip, an RCA CA3140, was chosen for its high input impedance (10^{12} ohms) and low input current (1×10^{-11} amperes, typical) and is connected as a high-input-impedance follower with adjustable gain. Power supply bypassing is provided at the amplifier by two 0.01-microfarad chips. A capacitor built into the thick film rolls the amplifier off at high frequency. Another capacitor is used to create a low-pass corner at 1000 Hz to reduce the resonant peaking. The last capacitor is used in the ac gain section. Fig. 6 is the accelerometer schematic.

The accelerometer characteristics are displayed in Fig. 7. An important characteristic not shown is thermal transient response. Because of pyroelectric effects and the low mass of the transducer, the thermal transient effect is excessive and requires stabilizing by thermal isolation and/or close thermal com-

munication with a large mass. This is achieved in the plotter by mounting the accelerometer close to the motor but separated from it by a plastic mounting frame. The magnitude of the pyroelectric effect is such that a temperature change of one degree celsius, experienced by a single plate of the sensor, produces a change in charge equivalent, in this design, to a 350-g signal. However, the beam is a sandwich of two oppositely poled plates, thereby reducing the effect to that from the mismatch in their individual pyroelectric properties. In the 7225A, additional insensitivity to this parameter is afforded by ac coupling of the ac-

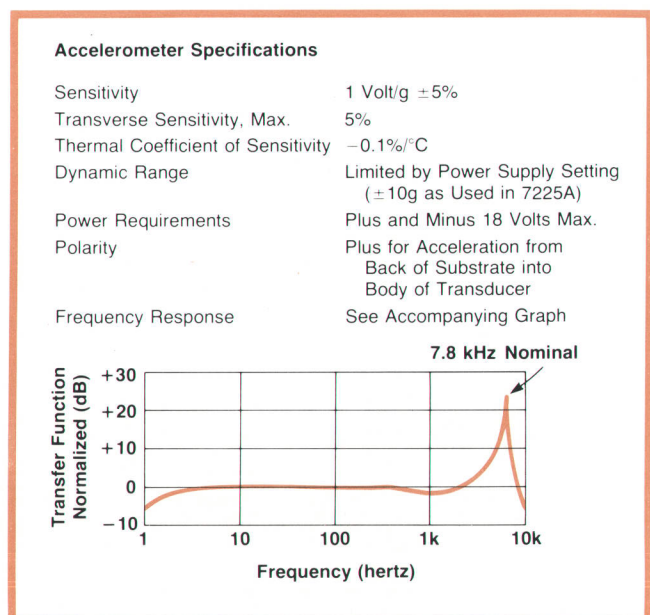


Fig. 7. Accelerometer characteristics.

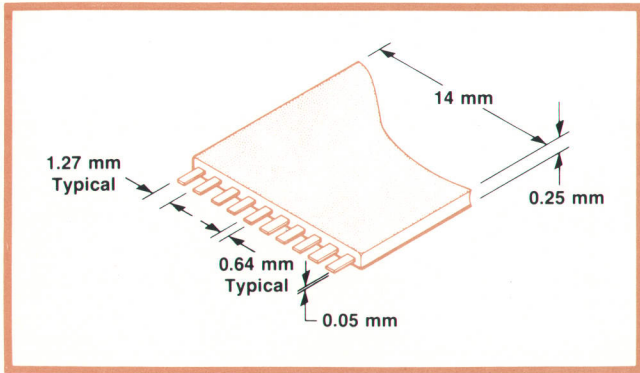


Fig. 8. Electric cable design for connecting the motor and accelerometer to the electronics section.

celerometer signal.

Electric Cables

The electric cable used to interconnect the motor, accelerometer, and pen lift (or Y limit switch) to the electronics section consists of ten flat conductors imbedded in polyester insulation (see Fig. 8).

The Y-motor cable is contained within the Y-arm cover and has a working diameter of forty millimetres. Tests were run to determine the fatigue life of the cable. Different diameters were used to generate a curve of fatigue life as a function of bend diameter (Fig. 9). Samples run at a forty-millimeter diameter indicate a flex life greater than five million cycles. It is interesting to note that all failures were gradual and marked by an increase in resistance that became more rapid and erratic with time, culminating in an open conductor. The X-motor cable has a much larger working diameter; therefore, cable life for the plotter is determined by the Y-motor cable. The X and Y cables are identical except for length.

Both ends of the cable are terminated by small printed circuit boards. In preparation, the cable end is stripped on both sides simultaneously by dual abrasive wheels. The bared (and cleaned) copper conductors are then fluxed, tinned, and then gang-reflow soldered to the printed circuit boards using a time and

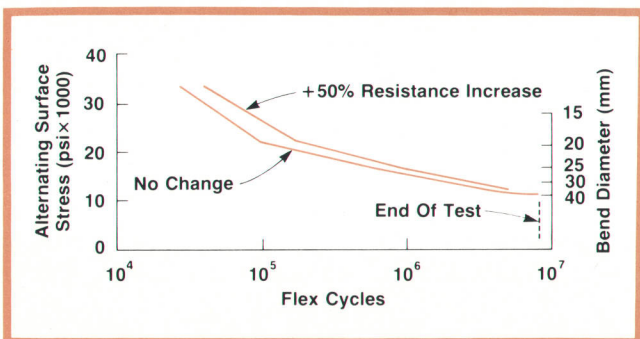


Fig. 9 Cables have a flex life greater than five million cycles.

temperature controlled resistance-heated low-mass bar.

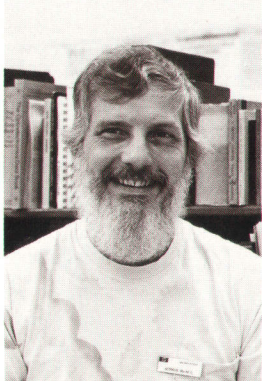
One board is used as a plug at the electronics interface. The other is used to connect to the motor windings, the accelerometer, and the pen lift or limit switch.

The Y motor, accelerometer, and pen-lift interconnection adds 6.5 millimetres to the length of the Y motor. The interconnection scheme uses a plastic frame to retain the accelerometer, cable printed circuit board, and connectors while aligning them to another board permanently attached to the motor. This board terminates the motor windings and the pen lift mounting bracket leads. The Y motor piece functions as pressure clamp, cable strain relief, and Y initializing switch actuator and is held in place with a single screw. The X-motor system is identical except for the metal piece, which performs only a clamping function and is held in place by two screws.



Philip P. Maiorca

An HP employee since 1972, Phil Maiorca was responsible for the servo work on the 7225A Plotter and contributed to the design of the 3964A and 3968A Instrumentation Tape Recorders. Phil received his BA degree in applied physics in 1971 from the University of California at San Diego and is expected to complete his MSEE degree from Stanford University by June 1979. Born in Los Angeles, California, Phil is single and is a resident of Poway, California. In his leisure time, he enjoys "dabbling in photography," playing baseball and ice hockey, and playing bridge.



Norman H. MacNeil

Norm MacNeil joined HP's Waltham Division in 1953 (then the Sanborn Co.), working primarily on transducers, pen motors, and ink regulators, and then transferred to HP's San Diego Division where he has worked on pens, ink squirting, and thermal writing. Designer of the accelerometer and trailing cable system for the 7225A Plotter, Norm is named inventor on three patents—one relating to thermal writing and two to transducers. An Arlington, Massachusetts, native, he attended the New England Conservatory of Music and Harvard University. Norm lives in Poway, California, is married with seven children, and spends much of his spare time playing the piano and violin, painting, bicycling, and restoring old cars.

Multi-Frequency LCR Meters Test Components under Realistic Conditions

Covering frequency ranges of 100 Hz to 100 kHz and 10 kHz to 10 MHz, these two new automatic LCR meters each provide up to twelve test signal frequencies, continuously variable test signal levels, and a wide choice of displayed parameters.

by Kohichi Maeda and Yoh Narimatsu

ADVANCES IN ELECTRONICS have created an increasing variety of electronic devices and circuit techniques. Along with these have come requirements for measurements of a wider array of parameters under a wider range of conditions.

The new HP Models 4274A and 4275A Multi-Frequency LCR Meters address this need, bringing a new measuring concept and functional elegance to component and circuit parameter measurements. This means that the measurement frequency, test level and dc bias voltage can be set very close to the actual working conditions of the device under test, and the result to be displayed can be chosen from among many parameters. Thus, the measurements most suitable and useful to the individual application are obtained.

Many of these measurements have been either not practical, very difficult, or very costly to make with earlier instruments that were designed to make mea-

surements only under relatively limited test conditions. For example, capacitance-versus-voltage or conductance-versus-voltage measurements are valuable in evaluating semiconductor wafers, chips, and the fabrication process. Output impedance measurements over a wide frequency range are essential in developing high-performance power supplies. Measurements at various test levels over a wide frequency range may be required in evaluating new electronic materials. Because of its level dependence, the inductance of a cored inductor should be measured at its actual working level. These are only a few of the measurement applications for which the new Models 4274A and 4275A LCR meters are suitable.

The 4274A and the 4275A, Fig. 1, are twins based on the same design philosophy. They basically have a 4½-digit display and can provide a 5½-digit readout in their high-resolution modes. Their three major features are multiple measuring frequencies, variable

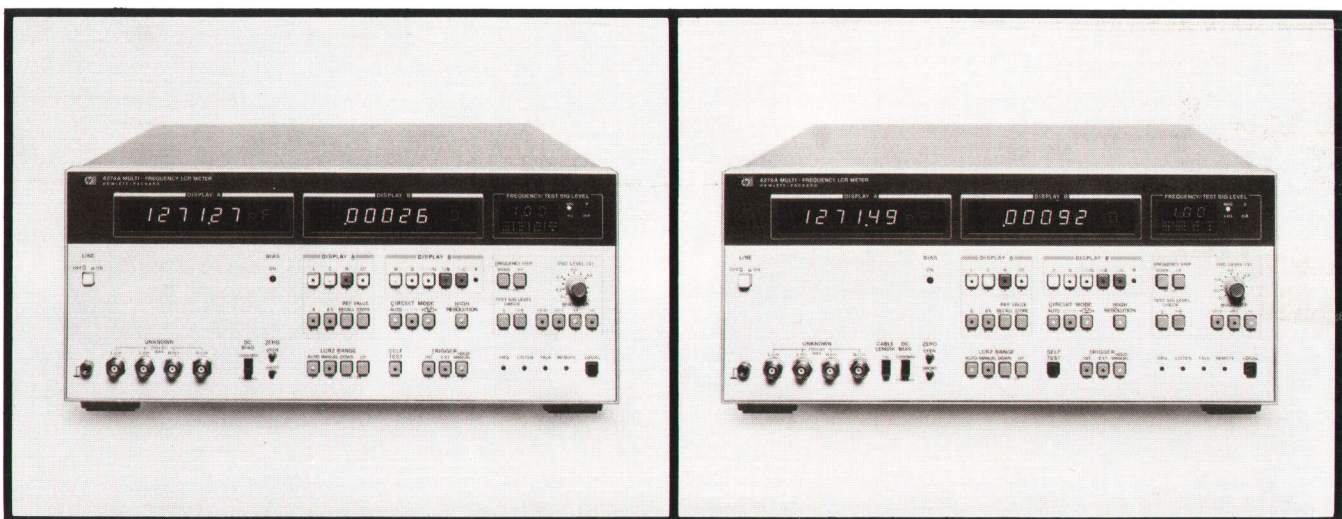


Fig. 1. Models 4274A (l) and 4275A (r) Multi-Frequency LCR Meters measure component values and circuit parameters at any of ten standard frequencies and two optional frequencies. Test signal levels and dc bias levels are also selectable. Model 4274A covers a frequency range of 100 Hz to 100 kHz while Model 4275A covers 10 kHz to 10 MHz. Both instruments have 4½-digit displays and can provide 5½-digit readouts in their high-resolution modes.

test signal and dc bias levels, and widely selectable measuring parameters.

The 4274A covers a measuring frequency range of 100 Hz to 100 kHz while the 4275A covers 10 kHz to 10 MHz. A test signal as low as 1 mV rms is selectable for low-level measurements. For higher levels, the maximum signal level of the 4274A is 5V rms, and for the 4275A, 1V rms. In addition to the usual measurement parameters, such as L, C, R, D and Q, both models provide readouts of other parameters convenient in some applications. Among these are impedance magnitude and phase, parallel admittance or capacitance, and series impedance or inductance.

Measurement accuracy depends on a state-of-the-art electronic automatic bridge technique and a newly developed 90-degree phase reference generator. A microprocessor controls the analog section that includes the bridge section and manipulates the data taken from the analog section to obtain the parameters to be displayed. All front-panel information and all front-panel controls (except for the test level vernier control) are accessible through HP-IB lines (IEEE 488-1975, ANSI MC1.1).

The Bridge Section

Fig. 2 is a simplified block diagram of the bridge section. The test signal is applied through dc bias isolation transformer T1. Current i_x flows into the DUT (device under test) via source resistor R_s , through reference resistor R_R (i_R), and returns towards T1 via a return path. The outer conductors of the H and L current coaxial cables form a part of this return path. At balance, the magnetic fields generated by the currents flowing in the inner and the outer conductors of the test leads cancel each other, so measurement errors caused by mutual inductance between the test leads can be avoided. This is one of the major advantages of the four-terminal-pair configuration shown in Fig. 2 over an ordinary four-terminal connection.

If the bridge is in an unbalanced condition, an error current i_d flows into the null detector, A1, and is amplified through several gain stages. The amplified error signal is fed back to the other side of the reference resistor until the system becomes balanced, that is, until i_d equals zero.

As the measurement frequency increases, various effects that introduce measurement errors begin to

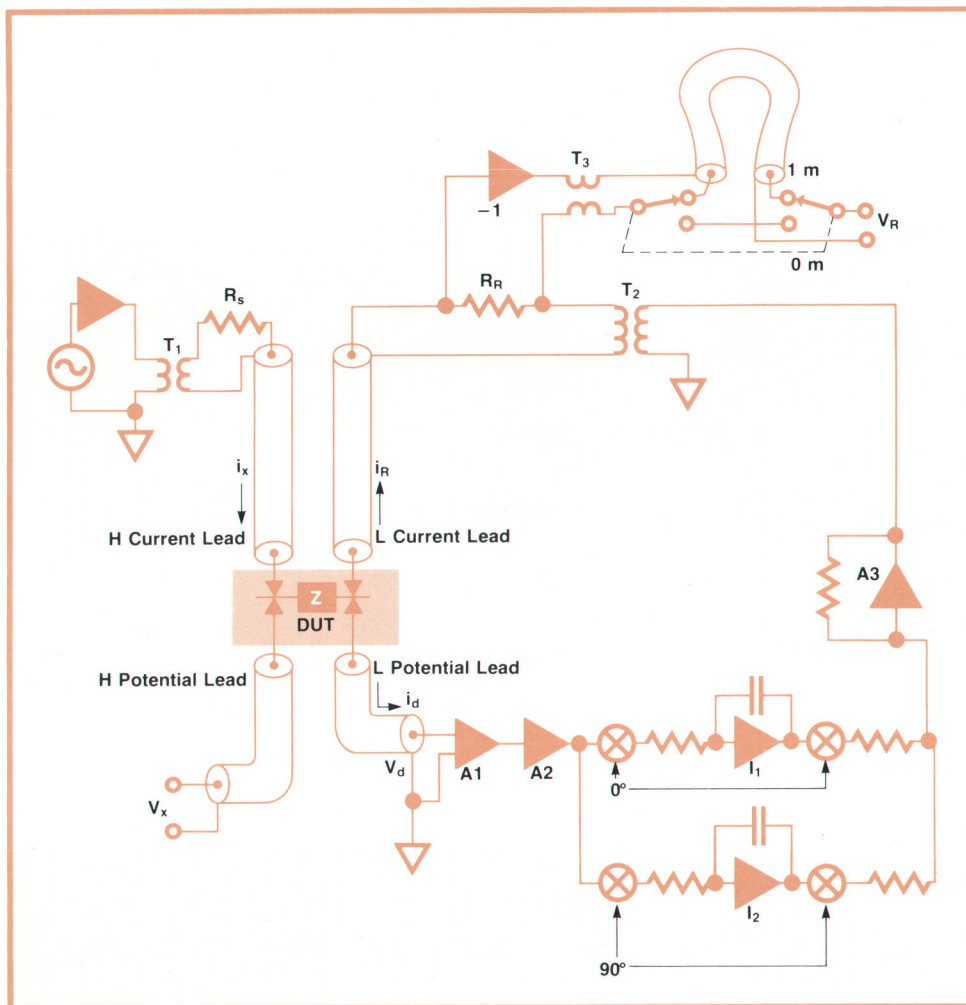


Fig. 2. A state-of-the-art electronic bridge system is used in the 4274A/4275A. Four-terminal-pair configuration eliminates measurement errors caused by mutual inductance between test leads.

appear. Among these are transmission effects of test leads, residual impedance at DUT contact points, common mode signals superposed on the outputs of the detector section, and undesirable signal leakage.

To compensate for the transmission effects of test leads, a cable length adjustment is provided between the bridge section and the vector ratio detector. A front-panel switch selects either 0 m or 1 m. This compensation is especially important above 1 MHz, and for this reason, *the lengths of test leads cannot be arbitrarily chosen*, since a measurement error of more than 30% could be introduced.

At balance, $i_d = V_d = 0$.

Then

$$\frac{V_x}{Z_x} = i_x = i_R = -\frac{V_R}{R_R}$$

Therefore,

$$Z_x = -R_R \frac{V_x}{V_R}$$

As may be seen from the above, all that is needed to calculate the complex impedance of the DUT are the values of R_R and the vector ratio (not the absolute values) of V_x and V_R . Therefore, the only component of the bridge section that is critical to accuracy is the range resistor R_R . However, the circuit techniques used in constructing the bridge section required considerable development because existing technologies were no longer applicable above 1 MHz. Careful attention was also paid to the associated circuit components, printed circuit board layout, and shielding.

The bridge must balance over a very wide frequency range for any DUT. One consequence of this is that the number of adjustments that have frequency dependence should be as few as possible. Otherwise

stable operation could not be expected for the optional frequencies, which cannot be known before manufacture. For this reason, an approach involving individual adjustments for each of the test frequencies is not employed. Only the 90-degree generator for the modulator and demodulator and the common mode rejection circuit in A3 (Fig. 2) require frequency decade control. This information is provided by the microprocessor.

The Vector Ratio Detector

The vector ratio detector detects the complex ratio (magnitude ratio and phase difference) of V_x and V_R .

V_x and V_R are buffered and then multiplexed so that the two signals can share the same amplification path and thus keep the tracking error between the two channels to a minimum (Fig. 3). Because the input signal level varies widely according to the test level, frequency, and DUT value, the signal-processing amplifier block has several attenuators and a variable-gain amplifier, along with fixed-gain amplifiers, to optimize the signal level to the phase detector. Assume, for example, that the DUT is a capacitor. When the test frequency doubles, the DUT impedance is halved, and consequently, V_x/V_R is also halved. If the DUT is an inductor the effect is the opposite. When the DUT is reactive, the gain when the multiplexer is switched to V_x is changed according to the test frequency. R_R is switched as the test frequency is changed and a 1/2 or 1/4 attenuator used as needed. These conditions provide an input ratio to the phase detector of almost unity, where the detector operates with highest accuracy.

The attenuators must provide accurate attenuation ratios, both magnitude and phase, up to 10 MHz, since any error here would contribute directly to measurement error. For this reason, careful construction

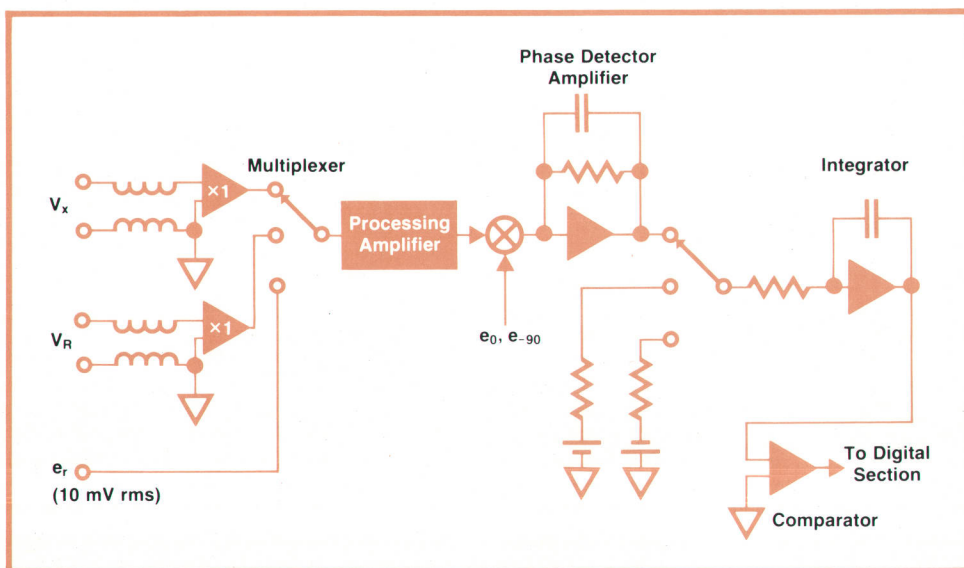


Fig. 3. Vector ratio detector measures the complex ratio of V_x and V_R .

is necessary. The linearity of each amplifier is also important, since a harmonic distortion of 0.1% can produce an error of more than 0.1% in the fundamental measuring signal components. To maintain such conditions over wide signal-level and frequency ranges required extraordinarily careful circuit design.

The 4274A and 4275A each have only one phase detector for detecting the vector ratio of the bridge outputs. The phase detector is timeshared to avoid errors that could possibly be introduced by differences in phase detection characteristics if multiple phase detectors were used. The detector is also designed to be insensitive to harmonic components of the test frequency, which might be introduced when a nonlinear component is tested.

To know the precise vector ratio of V_R and V_x , an accurate 90-degree phase difference is necessary as a phase reference (refer to Fig. 3). Suppose the input multiplexer is switched first to V_x . It is phase detected with respect to e_0 , which has a fixed (but not known) phase relationship to the test signal, and the output of the detector is $v_{x|0}$. The multiplexer is then switched to V_R and the output of the detector is now $v_{R|0}$. Again the multiplexer is switched back to V_x , and this time, the signal is phase detected with respect to a 90-degree lagging signal (e_{-90}) producing an output $v_{x|-90}$. Finally the multiplexer is again switched to V_R to produce an output $v_{R|-90}$.

An important point is that the actual phase relationship between the test signal and the phase detector reference signal does not have to be zero degrees or some other known value, although it should be

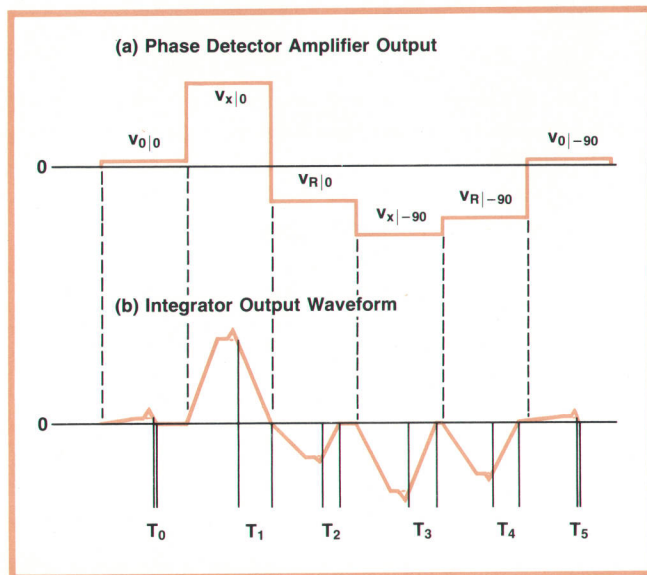


Fig. 4. Waveforms in the vector ratio detector of Fig. 3. The output waveform of the phase detector is integrated and converted to time periods proportional to the phase detector output during various measurement phases.

fixed. Besides $v_{x|0}$, $v_{x|-90}$, $v_{R|0}$, and $v_{R|-90}$, a phase detector output with the input multiplexer off ($v_{0|0}$) is necessary to remove the offset components included in these values. The offset value is detected with respect to both e_0 and e_{-90} and the phase detector

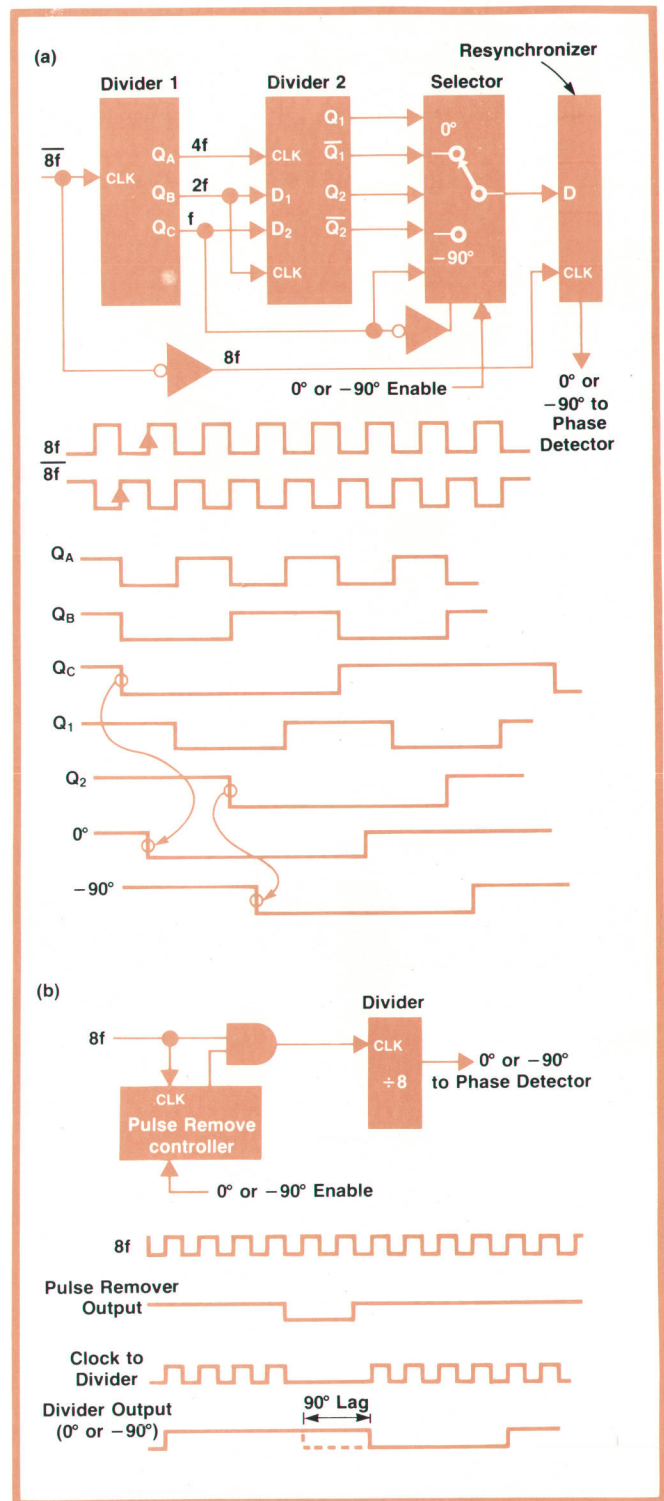


Fig. 5. An accurate 90-degree phase reference is required for accurate reactance measurements. (a) 4274A phase reference generator. (b) 4275A phase reference generator.

outputs are $v_{0|0}$ and $v_{0|-90}$, respectively. A dual-slope analog-to-digital converter converts these six analog values to digital signals, as shown in Fig. 4.

Reactance Standard Not Needed

As stated above, the only requirement for accurate reactance measurements is an accurate 90-degree difference between e_0 and e_{-90} . Since a dissipation factor D of 0.001 at 10 MHz, for example, requires detection of a phase difference as small as 16 picoseconds, reference phase generation is extremely critical.

The reference phase is generated using digital techniques. Figs. 5a and 5b show the reference generators for the 4274A and 4275A, respectively. Both circuits use a signal whose frequency is eight times ($8f$) higher than the test signal frequency (f) to produce a 90-degree difference for f . The 4274A uses a divider chain and gates to select the appropriate phase relationship between e_0 and e_{-90} .

A different approach is used in the 4275A. Since a difference in propagation delays in the selector causes a significant phase inaccuracy at higher frequencies, a pulse remover is employed. Two $8f$ pulses are removed to get e_{-90} after an e_0 phase detection has been completed. As the pulse removal control section does not affect the total propagation delay, e_0 and e_{-90} go through the same path and the 90-degree accuracy depends only on the short-term stability of $8f$ (which basically has quartz crystal stability).

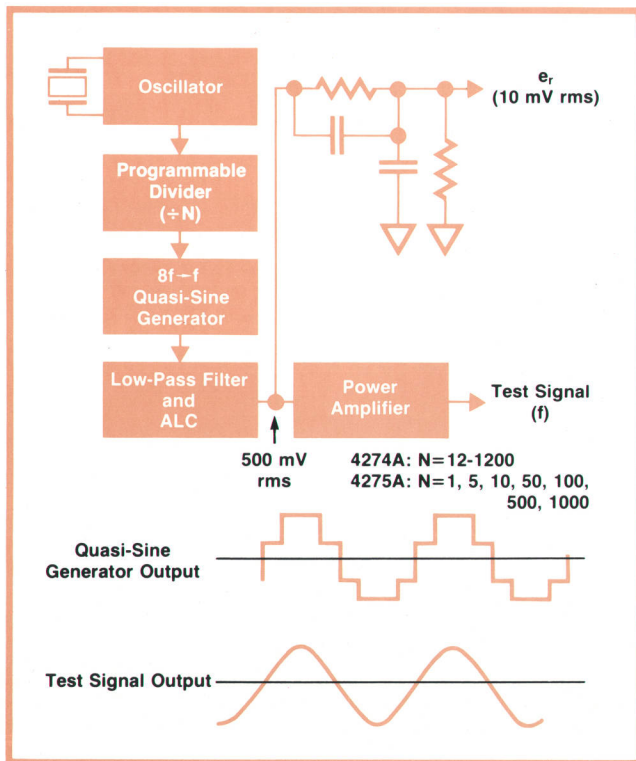


Fig. 6. Test and reference signals are generated in the signal source section.

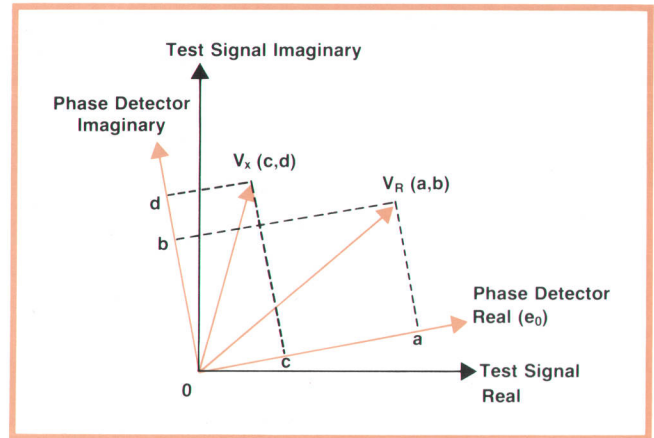


Fig. 7. Vector diagram showing components of V_x and V_R used in calculating the complex ratio of these two voltages.

The Signal Source Section

In impedance measurements, a good quality test signal is essential for obtaining accurate results. To generate the ten standard measuring frequencies from 100 Hz to 100 kHz in the 4274A, a 9.6-MHz quartz crystal and a frequency divider chain are provided. Two quartz crystals are incorporated to cover 10 kHz to 10 MHz in the 4275A, either a 32-MHz and an 80-MHz crystal or a 24-MHz and an 80-MHz crystal, depending upon the frequency step sequence (1-2-4 or 1-3-5). A maximum of two optional frequencies can be provided in addition to the ten standard frequencies, either by adding special division numbers in the divider chain or by putting in additional quartz crystals. The original frequency is divided down until the desired frequency is obtained. The signal is filtered to get a pure sine wave (Fig. 6).

Computations

All the information necessary to compute the desired parameters, including C , L , R , D , Q , and so on, are contained in the six time intervals, namely T_0 , T_1 , T_2 , T_3 , T_4 , and T_5 in Fig. 4. Fig. 7 is a vector diagram that explains how the vector ratio of V_x and V_R is calculated. Here a , b , c , and d are the vector components with a phase detector difference of zero degrees.

$$\frac{V_x}{V_R} = \frac{c+jd}{a+jb} = \frac{ac+bd}{a^2+b^2} + j \frac{ad-bc}{a^2+b^2}$$

$$= X + jY$$

where $X = \frac{ac+bd}{a^2+b^2}$

$$Y = \frac{ad-bc}{a^2+b^2}$$

Since V_R represents the vector impedance of the range resistor R_R , whose actual impedance is adjusted

to $R_R + j0$, the actual vector impedance of the device under test (Z_x) can be denoted as follows:

$$Z_x = -\frac{V_x}{V_R} R_R = -(X + jY)R_R$$

If, for example, the device under test is a series combination of a resistance R_x and an inductance L_x ,

$$Z_x = R_x + j\omega L_x = -(X + jY)R_R$$

Then, comparing both sides of the above equation,

$$R_x = -XR_R$$

$$L_x = -YR_R/\omega$$

where $\omega = 2\pi f$. Similarly, any unknown impedance can be calculated from X , Y , f and R_R .

The relationships between T_0 through T_5 and a through d are as follows:

$$a = T_2 - T_0$$

$$b = -(T_4 - T_5)$$

$$c = T_1 - T_0$$

$$d = -(T_3 - T_5)$$

T_5 is practically equal to T_0 if the measuring frequency is below 1 MHz, so only five measurement sequences are used at these frequencies.

The switching sequence shown in Fig. 4 is used when Z_x is somewhat smaller than R_s (50 ohms nominal for the 4274A, 100 ohms nominal for the 4275A). In this case V_x is proportional to the impedance of Z_x and, for convenience, the measurement is called an impedance measurement. When Z_x is greater than R_s , V_x is almost constant and V_R is proportional to the admittance of the device under test. Therefore, the measurement is called an admittance measurement, and the admittance of the DUT is calculated as follows:

$$Y_x = -\frac{V_R}{V_x} \cdot \frac{1}{R_R} = -(X + jY) \frac{1}{R_R}$$

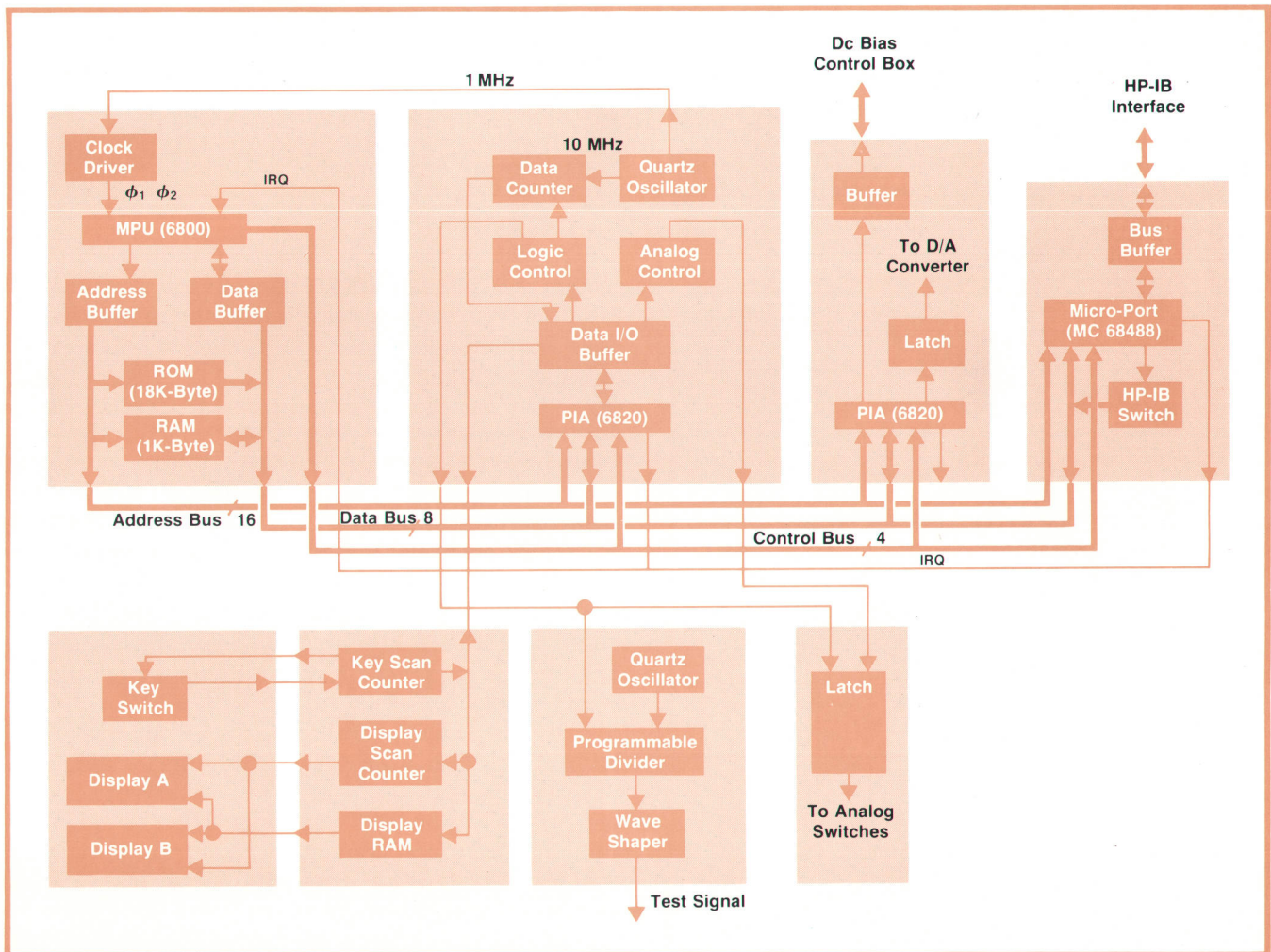


Fig. 8. Digital section block diagram. A 6800 microprocessor handles computation and control.

For an admittance measurement, X and Y are defined as:

$$X = \frac{ac+bd}{c^2+d^2}$$

$$Y = \frac{ad-bc}{c^2+d^2}$$

For simplicity, quantities x and y can be defined as:

$$\begin{aligned} x &= -XR_R && \text{impedance measurement} \\ y &= -YR_R \\ x &= -X/R_R && \text{admittance measurement} \\ y &= -Y/R_R \end{aligned}$$

where the negative signs are added to eliminate the effect of polarity inversion in the bridge. Conversion relationships between parameters to be displayed and x, y, and ω are listed in Table 1.

Effects due to the residual impedances of a test fixture can be automatically cancelled. The stray capacitance of a test fixture is digitally stored by pressing the OPEN button of the ZERO adjustment with the test fixture open. Residual inductance and resistance are stored by pressing the SHORT button with the test fixture shorted. These stored values are reflected in measurement calculations. If the optional memory back-up is installed, stored values are retained permanently even when the power switch is off.

Parameters To Be Displayed	Impedance Measurement	Admittance Measurement
C_p	$-\frac{1}{\omega y(1+D^2)}$	$\frac{y}{\omega}$
C_s	$-\frac{1}{\omega y}$	$\frac{y}{\omega}(1+D^2)$
L_p	$\frac{y}{\omega}(1+D^2)$	$-\frac{1}{\omega y}$
L_s	$\frac{y}{\omega}$	$-\frac{1}{\omega y(1+D^2)}$
$R_s(=ESR)$	x	$\frac{1}{x(1+Q^2)}$
R_p	$x(1+Q^2)$	$\frac{1}{x}$
D	$\frac{x}{ y }$	$\frac{x}{ y }$
Q	$\frac{ y }{x}$	$\frac{ y }{x}$
X_s	y	$-\frac{1}{y(1+D^2)}$
B_p	$-\frac{1}{y(1+D^2)}$	y
Z	$\sqrt{x^2+y^2}$	$\frac{1}{\sqrt{x^2+y^2}}$
θ	$-\tan^{-1} \frac{y}{x}$	$-\tan^{-1} \frac{y}{x}$

Table 1. Parameter Conversion Table

Test Level Readout

Test level monitoring is one of the features of the 4274A and 4275A. Because of the source resistance R_s , the actual test signal level across the DUT is different from the oscillator output level, especially when the DUT impedance is somewhat lower than R_s . A monitor readout displays the actual test level at the DUT.

The test signal voltage is calculated by taking the ratio of V_x to the absolute value of the reference voltage ($e_r = 10$ mV rms). The current flowing through the DUT (i_x or i_R in Fig. 2) can also be monitored. These values are calculated as:

$$|V_x| = \left| \frac{V_x}{e_r} \right| \cdot 10 \text{ mV}$$

$$|i_x| = |i_R| = \left| \frac{V_R}{e_r} \right| \frac{1}{R_R} \cdot 10 \text{ mV}$$

Precision dc Bias

Precisely settable dc bias is necessary for semiconductor tests, for example, and a relatively high voltage bias is usually necessary for evaluating electrolytic capacitors. Two types of optional dc bias supplies are available for the new LCR meters. One provides a bias range of 0 to ± 35 V, 40 mA maximum, and the other provides 0 to ± 99.9 V, 2 mA maximum. Voltage resolution is as low as 1 mV.

The Digital Section

Fig. 8 shows the overall block diagram of the digital section. All data and analog controls are managed by the M6800 microprocessor. Troubleshooting is easily done with the self-diagnosis capability, supplemented by signature analysis.

Acknowledgments

Models 4274A and 4275A are the results of team efforts. Team members who deserve special recognition are: Toshio Tamamura and Shigeru Tanimoto for the bridge section; Toshikuni Osogoe for the vector ratio detector section; Keiichi Yamamoto and Tomoyuki Akiyama for the signal source; Kiyoshi Suzuki for the power supply; Susumu Tokunaga, Takeshi Kyo and Kenzo Ishiguro for the digital section; Hideo Akama for the dc bias option; Yoshimasa Shibata for mechanical design; and Yoshio Sato for test fixtures. Industrial design was done by Kazunori Shibata. Thanks are due to Hiroshi Sakayori for preparing the calibration standards. Hitoshi Noguchi provided a ground framework. The products were designed and put into production under the general management of Masahide Nishida. We would like to thank Mitsutoshi Mori who gave much useful advice and encouragement to the team. Besides the above, many other people made significant contributions to

the project. Our thanks to them too. 

References

1. K. Maeda, "An Automatic, Precision 1-MHz Digital LCR Meter," Hewlett-Packard Journal, March 1974.
2. R.D. Cutkosky, "Techniques for Comparing Four-Terminal-Pair Admittance Standards", Journal of Research of the N.B.S., Vol. 74C, Nos. 3 and 4, July-Dec, 1970.



Kohichi Maeda

Kohichi Maeda received his BSEE from Waseda University, Tokyo, in 1963. Joining Yokogawa-Hewlett-Packard in 1964, he worked on the 4204A Digital Oscillator and the 4270A Automatic Capacitance Bridge, and designed the vector ratio detector section of the 4271A 1-MHz Digital LCR Meter. He was project leader of the 4261A LCR Meter before becoming project leader of the 4274A/4275A. Kohichi and his wife have three children. Playing tennis is his main recreation.



Yoh Narimatsu

Yoh Narimatsu joined Yokogawa-Hewlett-Packard in Tokyo, in 1971. After several years as a development engineer, he transferred to HP's Santa Clara Division and was involved in the 5342A Counter project. He designed the analog section for the 4275A LCR Meter, his first project after returning to Japan. Yoh holds a BSEE degree from Kyoto University and an MSEE from Stanford University. He enjoys playing volleyball and tennis in his spare time. He is married, and he and his wife have just had their first baby, a son.

APPENDIX

Effects of Test Leads and Test Fixtures on Measurement Accuracy

When long test leads or test fixtures are used at frequencies above 1 MHz, transmission effects of the test leads and residual inductances at the test fixtures can no longer be neglected. Although the 4274A and 4275A LCR Meters and their test fixtures are designed to keep these effects at a minimum, some degradation of the basic main-frame accuracy (see Specifications) may be introduced above 1 MHz.

Errors Due to Test Lead Transmission Effects

If the test lead length and the input capacitances of the bridge section and the vector ratio detector section are taken into account, the ratio of measured impedance to the true impedance of a DUT (device under test) is expressed as follows:

$$\frac{Z'_x}{Z_x} = \frac{\cos\theta_2}{\cos^2\theta_1} \frac{1 + jZ_0 Y_d \tan\theta_2}{1 + jZ_0 (Y_p + Y_d) \tan\theta_1}$$

where Z'_x = measured value of DUT impedance
 Z_x = true value of DUT impedance
 θ_1 = $2\pi/\lambda$ times test lead length
 (λ = wavelength at test frequency)
 θ_2 = $2\pi/\lambda$ times compensation cable length
 Z_0 = test lead characteristic impedance
 Y_p = input admittance for L current cable
 Y_d = input admittance for H potential cable
 (vector ratio detector input admittance)

In the 4274A and 4275A, θ_2 and Y_p are adjusted to bring the ratio Z'_x/Z_x to unity. However, when 1-m-long test leads are used, maximum errors of 5% in magnitude and 0.02 for dissipation factor are possible at 10 MHz. These errors are the result of adjustment inaccuracy and other effects related to the test lead length.

Errors Due to Test Fixture Parasitic Impedances

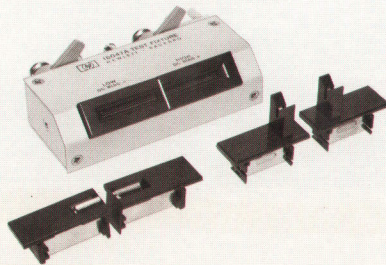
If parasitic impedances exist at the test fixture contact points for the H potential and L current leads, the ratio of measured to true impedances is as follows:

$$\frac{Z'_x}{Z_x} = 1 - Z_1 Y_d - Z_2 Y_p - j \frac{1}{Z_0} (Z_1 + Z_2) \tan\theta_1$$

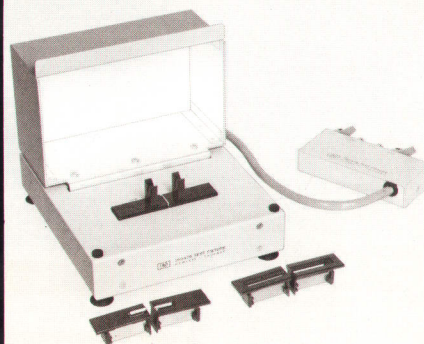
where Z_1 = residual impedance at H potential lead
 Z_2 = residual impedance at L current lead

The equation suggests that if test leads 1 m long are used, residual inductances of 30 nH at both contact points will cause an error of at least 1% in magnitude and 0.03 in dissipation factor at 10 MHz.

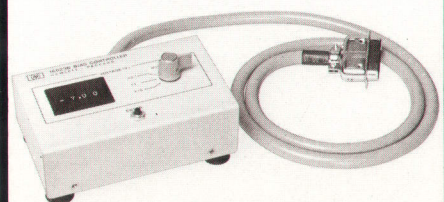
Residual inductances are introduced because the continuity of the cable characteristic impedance is disturbed at contact points, especially when the four-terminal contact configuration is used, as it is in the 16047A Test Fixture, for example. This effect can be significantly reduced if the Model 16047C Test Fixture is used and directly connected to the front panel, since the characteristic impedance of the 16047C is designed to be approximately 50 ohms.



16047A Test Fixture



16047B Test Fixture



16023B Bias Controller

SPECIFICATIONS

HP Models 4274A and 4275A Multi-Frequency LCR Meters

PARAMETERS MEASURED:

C-D / Q / ESR / G
 L-D / Q / ESR / G
 R-X / B / L / C
 $|Z|-\theta$

DEVIATION MEASUREMENTS:

Δ LCRZ and $\Delta\%$
 LCRZ difference from stored reference displayed in absolute value or percent.

TEST FREQUENCIES:

<p style="text-align: center;">4274A</p> <p>100 Hz-100 kHz in 1-2-4 steps and 120 Hz (100 Hz, 120 Hz, 200 Hz, 400 Hz, 1 kHz, 2 kHz, 4 kHz, 10 kHz, 20 kHz, 40 kHz, 100 kHz $\pm 0.01\%$) two additional frequencies available as an option 1-3-5 steps optional</p>	<p style="text-align: center;">4275A</p> <p>10 kHz-10 MHz in 1-2-4 steps (10 kHz, 20 kHz, 40 kHz, 100 kHz, 200 kHz, 400 kHz, 1 MHz, 2 MHz, 4 MHz, 10 MHz $\pm 0.01\%$) two additional frequencies available as an option 1-3-5 steps optional</p>
---	---

TEST SIGNAL LEVEL:

Continuously Adjustable	
4274A	4275A
1 mV to 5V rms	1 mV to 1V rms

MEASUREMENT RANGE AND BASIC ACCURACY:

PARAMETER	4274A		4275A	
	RANGE*	BASIC** ACCURACY	RANGE*	BASIC** ACCURACY
Inductance (L)	0.001 nH to 1999.9 H	0.1%	0.001 nH to 19.999 H	0.1%
Capacitance (C)	0.00001 pF to 1.999 F	0.1%	0.00001 pF to 199.99 μ F	0.1%
Resistance (R) Impedance (Z) Equivalent Series Resistance (ESR) Reactance (X)	0.001 m Ω to 19.999 M Ω	0.1%	0.01 m Ω to 19.999 M Ω	0.1%
Dissipation Factor (D)	0.00001 to 9.9999	0.001	0.00001 to 9.9999	0.001
Quality Factor (Q)	0.01 to 9900 (reciprocal display of D)		0.01 to 9900 (reciprocal display of D)	
Conductance (G) Susceptance (B)	0.00001 μ S to 199.99 S	0.1%	0.00001 μ S to 19.999 S	0.1%
Phase Angle (θ)	-180.00° to +180.00°	0.1°	-180.00° to +180.00°	0.1°

NOTES: *Varies depending on test frequency and test signal level.
 **Basic mainframe accuracy. Errors due to accessories may be significant at frequencies above 1 MHz and must be added to the basic mainframe accuracy. At frequencies above 2 MHz, the basic mainframe accuracy of the 4275A begins to roll off (e.g. 1% at 4 MHz, 2% at 10 MHz).

CIRCUIT MODE: Series, Parallel and Auto.

TEST TERMINALS: 4-terminal Pair Configuration.

DISPLAY: 5½ digit Display in High-Resolution Mode.
 4½ digit Display in Normal Mode.

ZERO ADJUSTMENT: For residual compensations
 Zero adjustment range: C \leq 20 pF, G \leq 5 μ S, L \leq 2 μ H, R \leq 0.5 Ω .

SELF-TEST: Automatic Operational Check

DC BIAS: Internal dc Bias (option)
 -35V to +35V 3 digit resolution (option 001)
 -99.9V to +99.9V 100 mV resolution (option 002)
 External dc Bias
 -200V to +200V

GENERAL SPECIFICATIONS

MEASUREMENT SPEED:
 4274A: 160 ms - 210 ms (100 Hz - 1 kHz)
 140 ms - 190 ms (1 kHz - 100 kHz)
 4275A: 140 ms - 190 ms
POWER: 100, 120, 220V $\pm 10\%$, 240V +5%-10%, 48-66 Hz
 Power Consumption 135VA max (4274A), 165VA max (4275A)
DIMENSIONS: Approx. 425.5 mm W \times 188 mm H \times 574 mm D (16.7 \times 7.4 \times 22.6 in.).
WEIGHT: Approx. 18 kg (39.7 lb).
OPTIONS: 001 Internal dc Bias -35V to +35V
 002 Internal dc Bias -99.9V to +99.9V
 003 Memory Battery Backup
 004 Measurement Frequency 1-3-5 steps
 101 HP-IB

SPECIAL: Two additional frequencies
FURNISHED ACCESSORY: 16047A Test Fixture, General-Purpose, Direct-Coupled

ACCESSORIES AVAILABLE:
 16047B Test Fixture, Safe Guarded with Extension Cable
 16047C Test Fixture, for High-Frequency Components
 16048A Test Leads, with BNC Connectors
 16048B Test Leads, with RF Connectors
 16048C Test Leads, with Alligator Clips
 16034B Test Fixture, for Chip Components
 16023B Dc Bias Controller

PRICES IN U.S.A.: 4274A, \$7930. 4275A, \$8720.
MANUFACTURING DIVISION: Yokogawa-Hewlett-Packard Ltd.
 9-1, Takakura-cho, Hachioji-shi
 Tokyo, Japan 192

Hewlett-Packard Company, 1501 Page Mill Road, Palo Alto, California 94304

**Bulk Rate
 U.S. Postage
 Paid
 Hewlett-Packard
 Company**

HEWLETT-PACKARD JOURNAL

FEBRUARY 1979 Volume 30 • Number 2

**Technical Information from the Laboratories of
 Hewlett-Packard Company**

Hewlett-Packard Company, 1501 Page Mill Road
 Palo Alto, California 94304 U.S.A.
 Hewlett-Packard Central Mailing Department
 Van Heuven Goedhartlaan 121
 Amstelveen-1134 The Netherlands
 Yokogawa-Hewlett-Packard Ltd., Suginami-Ku
 Tokyo 168 Japan

**Editorial Director • Howard L. Roberts
 Managing Editor • Richard P. Dolan
 Art Director, Photographer • Arvid A. Danielson
 Illustrator • Susan E. Wright
 Administrative Services, Typography • Anne S. LoPresti
 European Production Manager • Dick Leeksm**

0200032502&&&BARH&RLOO
 MR R L BARHAM
 GULF POWER CO
 PO BOX 1151
 PENSACOLA FL 32502

CHANGE OF ADDRESS: To change your address or delivery name from our mailing list please send us your old address label (it peels off). Send changes to Hewlett-Packard Journal, 1501 Page Mill Road, Palo Alto, California 94304 U.S.A. Allow 60 days.